

# Digital twin-driven energy consumption management of integrated heat pipe cooling system for a data center

Haitao Zhu, Botao Lin <sup>\*</sup>

*College of Information Science and Engineering / College of Artificial Intelligence, China University of Petroleum, Beijing 102249, China*

## HIGHLIGHTS

- A digital twin method on energy consumption management of cooling system is proposed.
- The digital twin models are developed for real-time monitoring and optimization.
- The approach has reduced the energy consumption of the cooling system by 23.63%.

## ARTICLE INFO

**Keywords:**  
 Digital twin  
 Energy consumption management  
 Cooling system  
 Real-time interaction  
 Genetic algorithm

## ABSTRACT

The energy consumption management (ECM) for the integrated heat pipe cooling (IHPC) systems has become a significant cost-cutting strategy, given the growing demand for the decreased cooling and maintenance costs in data centers. However, the traditional ECM strategies lack an integration with the real-time information and the automatic feedback control, causing the risks of system operation difficult to diagnose and the potential for energy saving hard to exploit. In this respect, a digital twin approach was proposed to efficiently and automatically implement the ECM strategy for an IHPC system. First, a digital twin architecture was established to enable seamless integration and real-time interaction between the physical system and the digital twin. Secondly, the digital twin models of monitoring, simulation, energy evaluation and optimization were developed to drive the corresponding services. Finally, the approach was verified on an IHPC system operating in a real-life data center. It is found that the approach can automatically detect and justify the abnormal states of the IHPC system. Moreover, the approach can reduce the power consumption by 23.63% while meeting the production requirements. The mean relative errors of the supply air temperature and the cooling capacity between the digital twin simulated and the on-site records are 1.43% and 1.46%, respectively. In summary, the proposed approach provides a digital twin workflow that can significantly improve the efficiency of the ECM strategy deployed on an IHPC system.

## 1. Introduction

The data centers have been widely constructed in recent years. The prevention of cooling system failures has led to research focusing on the real-time analysis, performance assessment, and health management of cooling systems [1]. Meanwhile, the cooling system brings up tremendous energy consumption. In a typical data center, the energy consumption of the cooling system accounts for >40% of the total electricity usage [2] [3]. Therefore, it is desirable to develop an efficient energy consumption management (ECM) method for the cooling system to decrease its energy consumption while reducing the risk of failure.

Currently, the cooling system type is predominantly based on air

cooling, whose ECM methods include design optimization and operation strategy optimization [4]. The integrated heat pipe cooling (IHPC) system is a popular air cooling system that combines the heat pipe indirect heat transfer method with the vapor compression refrigeration technique [5] [6]. An IHPC system typically consists of a heat pipe subsystem and one or more vapor compression sub-systems, as shown in Fig. 1. The operating mode changes with the outdoor temperature [5]. When the outdoor temperature is relatively low, the heat pipe subsystem works independently to provide the required cooling capacity for the data center. The heat pipe refrigerant is lifted by gas buoyancy from the evaporator to the condenser section and flows by gravity from the condenser to the evaporator section (Fig. 1). This mode is referred to

\* Corresponding author.

E-mail address: [linbotao@vip.163.com](mailto:linbotao@vip.163.com) (B. Lin).

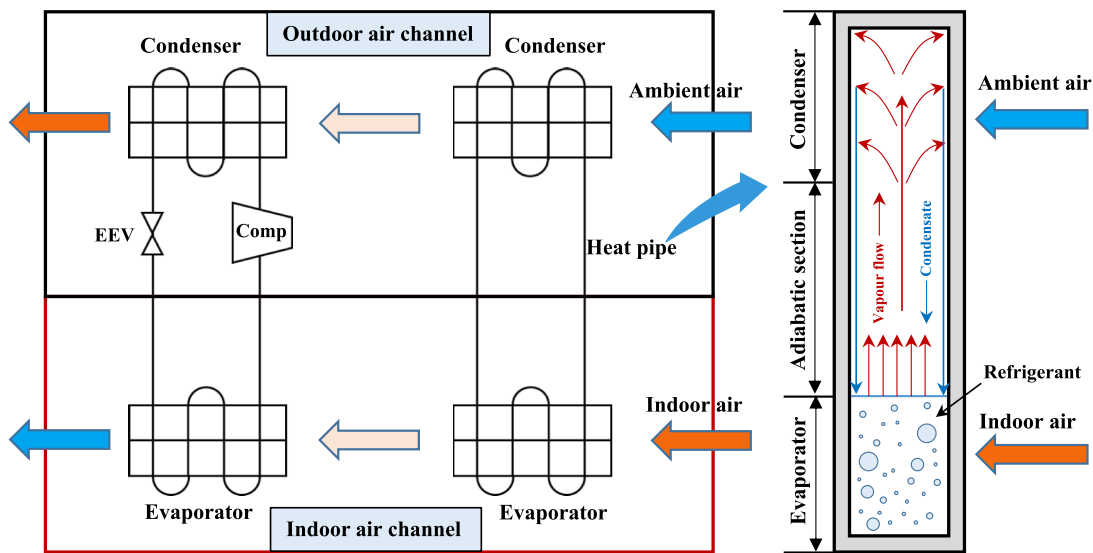


Fig. 1. Schematic diagram of the integrated heat pipe cooling system (Modified from the references [18,19]).

as free cooling as it uses the outdoor free cooling source without any external energy. When the outdoor temperature rises to the point that the heat pipe sub-system is not able to support the cooling demand, the compressor is turned on to activate the vapor compression sub-system. When the ambient temperature is above or equal to the indoor air temperature, the heat pipe sub-system stops working, while only the vapor compression sub-system operates to provide the required cooling capacity [7]. The working mode of the vapor compression sub-system is called mechanical refrigeration because it requires a compressor to provide power for circulating the working fluid. Typically, the working fluid in a heat pipe is selected according to its working temperature, which usually includes water, ammonia, and Freon [8]. Therefore, the IHPC system can conduct the year-round cooling for a data center regardless of the region and the climate [6]. Moreover, the system uses the outdoor cool air in an indirect manner, therefore reducing the energy consumption and avoiding the negative impact of the outdoor air quality on the data center environment [6]. However, regarding the operational strategy, most data centers operate with constant working parameters and at a low cooling efficiency [4]. The conventional ECM methods for the IHPC system are unable to apply real-time information to tackle the uncertainties of the system during its operation. They rely on the monitoring service but fail to consider the emergency cases and make subsequent adjustments. No integration with real-time information and a lack of automated feedback control hinder the emergency management and risk detection of the cooling system. Consequently, the existing ECM methods cannot respond immediately to any change in the cooling demand or the operating environment, leading to excessive energy consumption and high management costs.

The digital twin technology has been applied to efficiently integrate the physical assets and real-time information in several industrial sectors, for example, manufacturing [9], aerospace [10], maritime [11], construction [12], petroleum [13], and process industries [14]. The technology integrates several physical fields at multiple scales by synchronizing real-time data and mapping reality [15]. To date, both industry and academia have widely applied the technology to implement seamless connectivity between the physical and the virtual worlds, thereby providing new commercial opportunities across multiple sectors [16] [17].

In this regard, a digital twin approach was proposed for implementing the ECM of the IHPC system, which also includes the emergency management. To begin with, a digital twin architecture was constructed to enable seamless integration and real-time interaction between the physical twin and the digital twin. Afterward, the digital twin models on

monitoring, simulation, energy evaluation, and energy optimization were developed to perform the digital twin services. In particular, the emergency management of the IHPC system was integrated into the simulation model. Finally, each component in the architecture was implemented on a realistic cooling system running in a data center located in Shanghai, China, for which its feasibility and effectiveness were demonstrated.

The remainder of this paper is organized as follows: Section 2 reviews the ECM of the air-cooling system, the digital twin, and its application on industrial equipment. Section 3 presents the digital twin architecture for the ECM application on the IHPC system. Section 4 describes the digital twin modeling process. Section 5 illustrates the background of the case study and the deployment of the digital twin approach, closed by the discussion of results and conclusions in Section 6.

## 2. Literature review

This section reviews the ECM of the air-cooling system, digital twin, and its application on industrial equipment.

### 2.1. ECM of the air-cooling system

The ECM is critical to the operational efficiency and safety of the cooling system, which can reduce unplanned downtime and energy consumption while satisfying the cooling requirements. Dai et al. [1] assessed and mitigated the reliability risks of the equipment cooled by free air using the prognostics and health management (PHM) methodology, which was based on the operational characteristics of the data center. Wang et al. [20] used Long Short-Term Memory (LSTM) to predict the operational and abnormal states of the cooling equipment. To improve the energy efficiency of the cooling system, Oh et al. [21] proposed an optimization framework linking the process simulator and the external optimization method. The case study demonstrated that the energy consumption of the cooling system was reduced by 16.3–27.2% through the optimization of the refrigerant type and operating conditions. Du et al. [22] developed a generic energy management system for the large cooling system in deep mining wells. The field tests on four large cooling devices of various designs, sizes, and requirements resulted in an average saving of 33.3% on power consumption for all sites while fulfilling the cooling needs. To manage the energy consumption of heating, ventilation, and air conditioning (HVAC) equipment in buildings, Fong et al. [23] proposed a coupled metaheuristic simulation

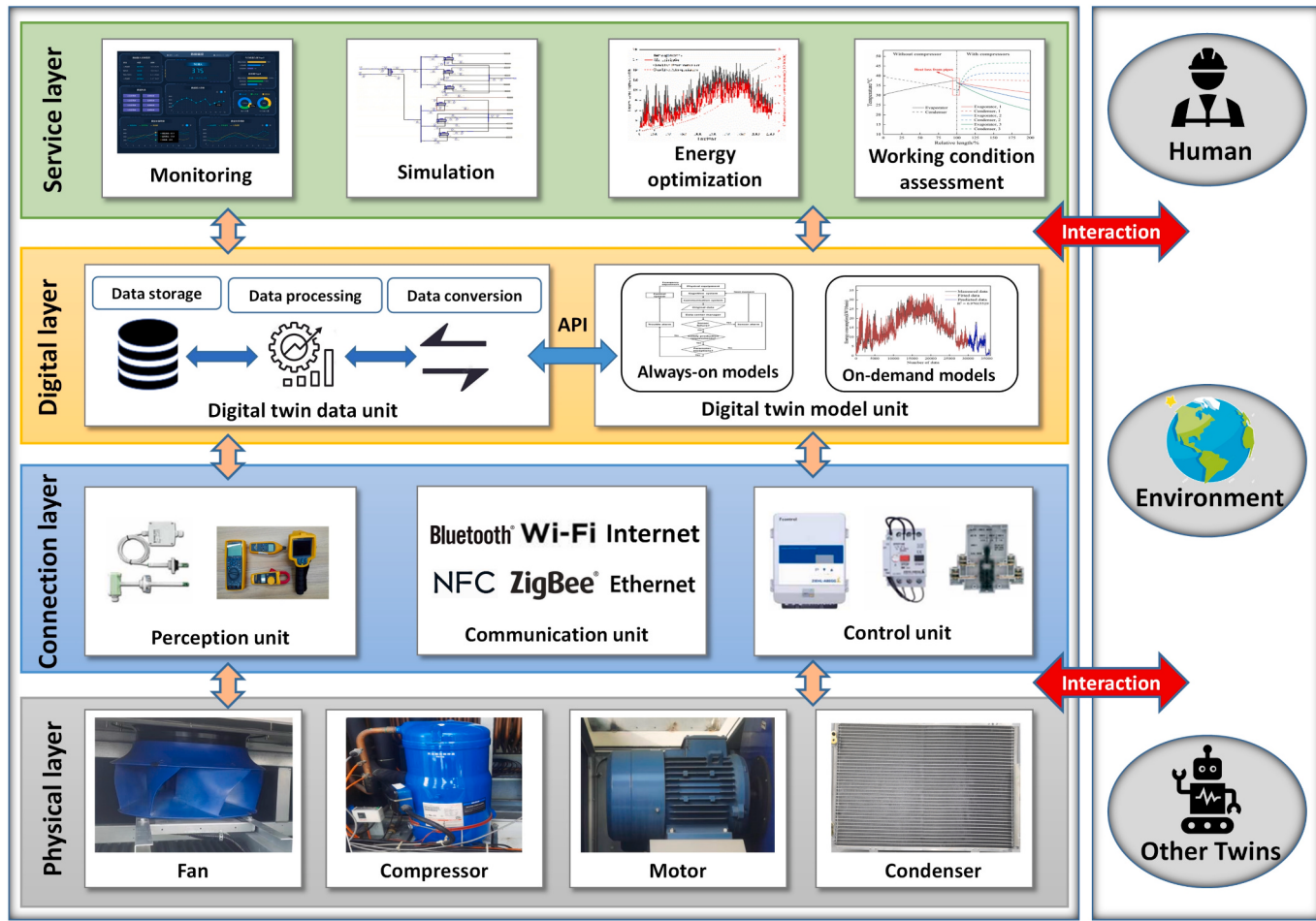


Fig. 2. ECM digital twin architecture for an IHPC system

method based on evolutionary programming. The simulation results showed that the method saved about 7.0% of the potential cost compared to the existing operational setup. Recently, the power usage effectiveness (PUE) has become one of the most critical indicators for evaluating the power utilization efficiency of a data center, which is defined as the ratio of the total power consumption of the data center to that of the IT equipment [6]. Given that the energy consumption of the cooling system can account for >40% of the total energy consumption of a data center, minimizing the former becomes crucial in reducing the PUE. To minimize the energy consumption of the cooling system, He et al. [2] obtained the optimal inlet temperature and water flow rates at different ambient temperatures using the fitting method. They conducted a case study using offline temperature data from Tianjin, China, which resulted in a 21.3% reduction in energy consumption and a decrease in average annual PUE from 1.263 to 1.207. He et al. [5] calculated the optimal operating parameters of an IHPC system at different outdoor ambient temperatures based on a genetic algorithm. They analyzed the energy-saving effect of the method using the offline temperature data in locations with different climates, and the optimized PUE was reduced by 16.2% compared to the PUE required by the local policy.

In summary, the existing ECM methods for the air-cooling system are primarily offline or dependent on historical data. In addition, the absence of integration with the automated control modules requires maintenance crews to stay on site. Moreover, the methods cannot respond to rapid changes in either the operating environment or the cooling demand of the data center, resulting in delayed emergency management and unnecessary energy consumption.

## 2.2. Digital twin and its application on industrial equipment

The concept of the digital twin was first introduced by Grieves in 2002 in a product lifecycle management (PLM) course [24]. Despite the increasing enthusiasm for digital twin among researchers in recent years, the concept of digital twin requires a more specific definition because the definitions and concepts mainly depend on their corresponding fields of application [25]. Kritzinger et al. [9] illustrated that the digital twin is distinguished from the digital model or the digital shadow in that it reveals the automatic real-time data interaction between the physical entity and the virtual twin. Meanwhile, the latest published international standards for digital twins define a digital twin as a digital representation of a target entity through a data connection that enables convergence between the physical and digital states at an appropriate synchronization rate [26]. It must be noted that the conventional numerical simulations are usually offline and consequently lack specific synchronization and feedback characteristics compared to a digital twin [26].

Several researchers proposed a digital twin model based on a fuzzy inference system to optimize the number of fans in the water-cooling system of a power plant [27]. Tao et al. [28] studied the PHM of complex equipment, developed a five-dimensional digital twin model, and proposed a digital twin-driven PHM approach. The method effectively used the interaction mechanism and fused data of a digital twin. Nguyen et al. [29] proposed a digital twin model for the system-level fault detection and diagnosis on a physical entity to improve the monitoring efficiency of the equipment health. The fault diagnosis of a high-pressure feedwater system was analyzed, and the system effectiveness was

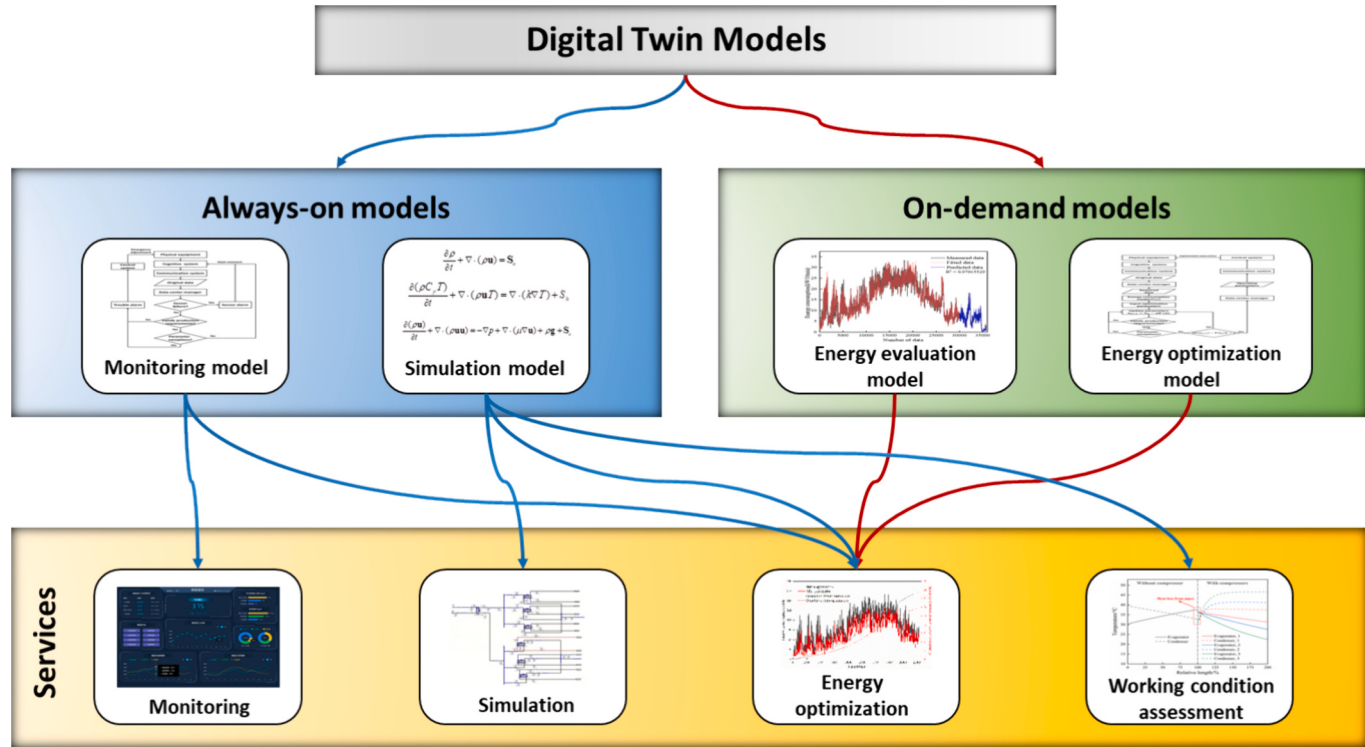


**Fig. 3.** Digital twin models and their relationship with the digital twin services.

proved. Ren et al. [30] introduced a technical system that integrates machine learning modules into a digital twin model, which was applied to the predictive maintenance of an internal combustion engine. The results showed that the bearing temperature anomalies in the internal combustion engine could be predicted one week in advance. Wei et al. [31] presented a multi-domain, multi-level, parametric, and consistent process to construct the mechanism-oriented digital twin model for a mechatronic device. The reliability of the method was verified by constructing a digital twin model of a computer numerical control machine.

In summary, the full integration of the physical and virtual models can improve the ECM efficiency for industrial equipment. However, there has been no application of a digital twin to the ECM method for the IHPC system in a data center. This study is aimed at tackling such an application.

### 3. Architecture of the digital twin approach

This research proposes an ECM digital twin architecture for the IHPC system based on the standard architecture according to the international standard ISO 23247-2 [32] and the five-dimensional model developed by Tao et al. [28], as shown in Fig. 2. The architecture is designed to guide and enable seamless integration and real-time interaction between physical and digital devices to improve the efficiency of the ECM. The architecture comprises five parts: a physical, a connection, a digital, a service, and an interaction layer. The devices in the physical layer are the main components of the IHPC system, which are connected in the digital layer via the perception, communication, and control units in the connection layer. The digital twin models located in the digital layer drive the services in the service layer to enable the automatic ECM of the IHPC system. The digital twin data unit in the digital layer manages and processes all the data generated by the digital twin and physical entities. This layered architecture follows the separation of concerns and allows for a high degree of modularity and reusability, showing improved scalability and reducing the developmental complexity of the digital twin [33,34]. The details of the architecture will be presented layer by layer in the following subsections.

- Physical layer

The physical layer performs as the cornerstone of the architecture and the service target entity of the digital twin. The physical layer contains the IHPC system components deployed in the physical world, such as fans, compressors, and motors. These physical equipment supplies the corresponding data to the digital twin via the perception unit in the connection layer. These data include the equipment geometry, physical properties, material parameters, structural composition, and real-time data generated from the system operation. It is worth noting that the physical layer needs to provide the key parameters to the ECM services, including the heat pipe size, refrigerant component, fan speed, and energy consumption. Such a setup can significantly reduce the data volume during the operation of the digital twin. The optimization signals are transmitted to the physical devices through the communication and control units in the connection layer to enable the digital twin functionality.

- Connection layer

The connection layer consists of a perception, a communication, and a control unit. The perception unit contains pressure sensors, temperature sensors, electric meters, and tachometers that record the data required for the digital twin modeling. The communication unit allows the components within the digital twin to exchange data to perform specific tasks. It transfers data from multiple sources obtained by the perception unit to the digital twin data unit. The optimization orders are then generated by the digital twin models and transmitted to the control unit that seamlessly integrates the physical and digital entities. For example, when the cooling demand cannot be met, the digital twin models output optimized IHPC operation orders (e.g., turn on more compressors or increase the speed of the fans) and transmit them to the control unit via the communication unit. The control unit then executes the operation orders and controls the physical IHPC system, which provides continuous feedback to subsequent adjustments such that the autonomous decision-making is fulfilled.

**Table 1**  
Notation in Algorithm 1 and Algorithm 2.

Notation	Remark	Notation	Remark
$E_i$	ith cooling equipment	$T_{s, \max}$	Max temperature of the supply air
$EF_{ij}$	jth evaporator fan of $E_i$	$T_r$	Temperature of the return air
$CF_{ij}$	jth condenser fans of $E_i$	$T_{r, \max}$	Max temperature of return air
$C_{ij}$	jth compressor of $E_i$	$TC_{ij}$	jth compressor back temperature of $E_i$
$S_i$	Status of $E_i$	$TC_{\max}$	Max back temperature of the compressor
$RE_{ij}$	rpm of jth evaporator fan of $E_i$	$PC_{ij}$	jth compressor pressure of $E_i$
$RC_{ij}$	rpm of jth condenser fan of $E_i$	$PC_{\max}$	Max pressure of the compressor
$S_{ij}$	Status of jth compressor of $E_i$	$T_o$	Outdoor temperature
$T_s$	Temperature of the supply air	$P_e$	Total power of the device
$t$	Data collection time interval	$\{S\}_i$	Dataset measured at moment i

- Digital layer

The digital layer includes a digital twin data and a digital twin model unit. It has been widely acknowledged that poor data quality is a highlighted problem in a noisy industrial environment [35], as the accuracy of the data model depends heavily on the quality of the input data. The digital twin data unit performs the data storage, processing, and conversion functions to obtain high-quality data. In this study, the digital twin models are encapsulated as always-on and on-demand models, which are defined based on their roles in driving the digital twin services. The relationship between the digital models and the services is given in Fig. 3.

- Service layer

The service layer lies at the top of the architecture and contains monitoring, simulation, energy optimization, and working condition assessment services. Each digital twin service is driven by one or more digital twin models, as depicted in Fig. 3. The monitoring service displays the operational status of the IHPC system in terms of curve-type

evaluation and optimization models. The developmental procedure of these models will be interpreted in Section 4.

- Interaction

A digital twin shall contain the appropriate interfaces for interaction with the outside world to avoid isolated digital islands. The interaction among the layers within a digital twin is executed through the application programming interfaces (APIs) and the perception, communication, and control units in the connection layer. The objects of interaction between the digital twin and the external include the human, the environment, and other twins. Among them, the interaction between the digital twin and the human requires visualization techniques to improve its efficiency. The interaction between the digital twin and the environment is achieved through the temperature sensors because the outdoor temperature has a significant impact on the operational status of the IHPC system. The interaction between the digital twin and other twins is conducted via an API.

## 4. Digital twin modeling

### 4.1. Monitoring model

The conventional ECM methods are absent of integration with the automation control and the emergency treatment. In this regard, a monitoring model was built to monitor the working status, detect abnormalities, and respond to emergencies. The model mainly consists of one algorithm for sensor failure detection and the other for abnormal working condition management.

**Algorithm 1** presents the detailed pseudo-code of the sensor failure detection algorithm, with the notation given in Table 1. The input is the real-time dataset  $\{S\}_i$ , describing the operating status of the IHPC system collected by the sensors. The output is the sensor failure information. For example, when the data collected by sensor 3 in cooling device 1 are absent, the output message of the algorithm reads “sensor 3 in device 1 has failed”. In this case, the alarm message is generated to remind the operator to maintain or replace the failed sensor (sensor 3 in device 1). The procedure first loops through the real-time dataset  $\{S\}_i$  of the operating status of all the activated devices, then detects whether they are void of data.

**Algorithm 1**  
Sensor failure detection algorithm.

---

**Input:** The real-time dataset  $\{S\}_i$  of the operating status of the equipment collected by the sensors  
**Output:** The sensor failure information

```

1: for i :=1 to num(Equipment) // Obtaining the working status of all equipment
2:   if  $S_i$  is True
3:     for  $S_{ij}$  in  $\{S\}_{ij}$ : // Looping through the sensor real-time dataset
4:       if  $S_{ij}$  is empty
5:         Send message (' $S_{ij}$  sensor failure')
6:       end if
7:     end for
8:   end if
9: end for

```

---

graphs of the key operating parameters, which are the supply and return air temperatures, fan speed, energy consumption, and compressor pressure. The simulation service simulates the process of IHPC system operation and predicts the key operating parameters such as the supply air temperature, cooling capacity, and energy consumption. These parameters are also used to assess the equipment responses under different outdoor ambient temperatures. The energy optimization services are implemented by combining the monitoring, simulation, energy

**Algorithm 2** provides the detailed pseudo-code to present the algorithm on the abnormal working condition management. The input data are the real-time dataset  $\{S\}_i$  collected by the sensors, and the threshold values. The outputs are abnormal alarm messages and adjustment measures. The procedure is designed as follows: 1) loop through the operating status of all the devices and issue the corresponding alarm when the cooling needs are not satisfied; 2) following the order of energy consumption from the smallest to the largest, increase the speeds of the

evaporator fan and the condenser fan, activate more compressors, and activate more cooling equipment until the demand for refrigeration suffices; 3) issue an alarm when either the compressor pressure or the compressor back temperature exceed the corresponding threshold. Shut down the warned compressor and turn on other compressors to ensure the health of the former. The alarm messages are employed to inform the operator about the location and the reasons for the anomalies, as well as to generate request for maintenance of the abnormal device.

#### Algorithm 2

##### Abnormal working condition management.

---

**Input:** The real-time dataset  $\{S_i\}$  collected by the sensors, and the threshold values

**Output:** Abnormal alarm messages and adjustment measures

```

1: for i :=1 to num(Equipment) // Looping through the working status of all equipment
2:   if  $S_i$  is True
3:     for j :=1 to num(EF) // Looping through the working status of all fans
4:       while  $T_s \geq T_{smax}$  &  $RC_{ij} < RC_{max}$  do
5:         Send message (' $T_s$  is too high')
6:          $RC_{ij} += 0.01 \times RC_{max}$  //Increase the condenser fan speed by 1 % each time
7:       end while
8:       while  $T_r \geq T_{rmax}$  & ( $RC_{ij} < RC_{max}$  or  $RE_{ij} < RE_{max}$ ) do
9:         Send message (' $T_r$  is too high')
10:         $RC_{ij} += 0.01 \times RC_{max}$  or  $RE_{ij} += 0.01 \times RE_{max}$ 
11:       end while
12:     end for
13:     for j :=1 to num(compressors) // Looping through the working status of all compressors
14:       while  $T_s \geq T_{smax}$  &  $S_{ij}$  is false do
15:         Send message (' $T_s$  is too high') &  $S_{ij}$  is True //Activating the compressor
16:       end while
17:       if  $S_{ij}$  is True
18:         if  $TC_{ij} \geq TC_{max}$  or  $PC_{ij} \geq PC_{max}$ 
19:           Send message (' $TC_{ij}$  or  $PC_{ij}$  is too high') and  $S_{ij}$  is false //Turn off the
            compressor
20:           for k :=1 to num(compressors)
21:             if  $S_{ik}$  is false and  $S_{ij} \neq S_{ik}$ 
22:                $S_{ik}$  is True // Activate another compressor
23:             end if
24:           end for
25:         end if
26:       else:
27:         while  $T_s \geq T_{smax}$  or  $T_r \geq T_{rmax}$  do
28:            $S_i$  is true //Activate more cooling equipment
29:         end if
30:       end for

```

---

#### 4.2. Simulation model

The simulation model is used to simulate the processes of fluid flow and heat transfer in the circulating channel during the operation of the IHPC system. During the circulation, the air flows through the channels at the condenser and evaporator, exchanging heat with the heat released from the phase change of the refrigerant inside the evaporator and

condenser tubes. In the simulation, the IHPC system contains indoor and outdoor air channels, heat pipe sub-system, and vapor compression sub-system (Fig. 1).

##### (1) Indoor and outdoor air channels.

Assuming that the airflow in the channel is one-dimensional, the governing equations of its flow process be expressed by Eq. (1)–(3). The mass conservation equation for the air flow in the indoor and outdoor channels in a unit control volume can be described by:

$$\frac{\partial \rho_a}{\partial t} + \nabla \cdot (\rho_a \mathbf{u}) = 0 \quad (1)$$

where  $\rho_a$  is the density of air,  $\text{kg/m}^3$ ;  $\mathbf{u}$  is the flow rate of the air,  $\text{m/s}$ ;  $t$  is time,  $\text{s}$ . The first term on the left part of Eq. (1) represents the change rate of the air mass per unit channel volume; the second term is the mass

flow rate of the air entering or exiting the unit area in the flow direction.

The momentum conservation equation for the air flow in a unit control volume is given by:

$$\frac{\partial(\rho_a \mathbf{u})}{\partial t} + \nabla \cdot (\rho_a \mathbf{u} \mathbf{u}) = -\nabla p_a + \nabla \cdot (\mu_a \nabla \mathbf{u}) + \rho_a \mathbf{g} \quad (2)$$

where  $p_a$  is the pressure in the air channel, Pa;  $g$  is the acceleration of gravity,  $\text{m/s}^2$ ;  $\mu_a$  is the dynamic viscosity of the air,  $\text{Pa}\cdot\text{s}$ . The first term on the left side of Eq. (2) represents the change rate of the air momentum per unit channel volume; the second term denotes the transport of the air momentum in the flow direction caused by convection. The first term on the right of Eq. (2) is the change in air momentum because of the pressure gradient; the second term characterizes the diffusion of momentum due to the viscous force within the air; the third term expresses the effect of gravity on momentum per unit volume of air.

The energy conservation equation for the air flow in a unit control volume is written by Eq. (3):

$$\frac{\partial(\rho_a C_a T_a)}{\partial t} + \nabla \cdot (\rho_a \mathbf{u} T_a) = \nabla \cdot (k_a \nabla T_a) + S_h + S_v \quad (3)$$

where  $T_a$  is the air temperature,  $^\circ\text{C}$ ;  $C_a$  is the specific heat capacity of air,  $\text{J}/(\text{kg}\cdot^\circ\text{C})$ ;  $k_a$  is the thermal conductivity of air,  $\text{W}/(\text{m}\cdot^\circ\text{C})$ ;  $S_h$  and  $S_v$  are the energy source terms contributed by the heat pipe and the vapor compression sub-system, respectively,  $\text{W}/\text{m}^3$ . The first term on the left of Eq. (3) is the change rate of energy per unit volume of the air; the second term represents the transfer of the air energy in the flow direction due to convection. The first term on the right shows the energy diffusion due to heat conduction;  $S_h$  and  $S_v$  represent the energy source terms of a unit volume of air due to the contribution of the heat pipe sub-system and the vapor compression sub-system, respectively.

## (2) Heat pipe sub-system

The VOF (Volume of Fluid) model can be employed to describe the phase change and flow of the refrigerant in the heat pipe sub-system [36,37]. The model is used to simulate two or more immiscible fluids by solving a set of momentum equations and tracking the volume fraction of each fluid in the domain [37]. The circulation of refrigerant in the heat pipe is a two-phase flow process. In each control volume, the sum of the volume fractions of all phases is 1, as shown in Eq. (4):

$$\alpha_v + \alpha_l = 1 \quad (4)$$

where  $\alpha_v$  and  $\alpha_l$  are the volume fraction of the vapor phase and the liquid phase, dimensionless.

The properties of the fluid in each control volume are the weighted sum of the properties of the individual phases:

$$\mu = \alpha_v \mu_v + \alpha_l \mu_l \quad (5)$$

$$k = \alpha_v k_v + \alpha_l k_l \quad (6)$$

$$\rho = \alpha_v \rho_v + \alpha_l \rho_l \quad (7)$$

$$C = \frac{\alpha_v \rho_v C_v + \alpha_l \rho_l C_l}{\alpha_v \rho_v + \alpha_l \rho_l} \quad (8)$$

where  $\mu_v$  and  $\mu_l$  are the dynamic viscosity of the vapor and the liquid phases,  $\text{Pa}\cdot\text{s}$ ;  $\mu$  is the dynamic viscosity of the mixed fluid,  $\text{Pa}\cdot\text{s}$ ;  $k_v$  and  $k_l$  are the thermal conductivity of the vapor and the liquid phases,  $\text{W}/(\text{m}\cdot^\circ\text{C})$ ;  $k$  is the thermal conductivity of the mixed fluid,  $\text{W}/(\text{m}\cdot^\circ\text{C})$ ;  $\rho_v$  and  $\rho_l$  are the density of the vapor and the liquid phases,  $\text{kg}/\text{m}^3$ ;  $\rho$  is the density of the mixed fluid,  $\text{kg}/\text{m}^3$ ;  $C_v$  and  $C_l$  are the specific heat capacity of the vapor and the liquid phases,  $\text{J}/(\text{kg}\cdot^\circ\text{C})$ ;  $C$  is the specific heat capacity of the mixed fluid,  $\text{J}/(\text{kg}\cdot^\circ\text{C})$ .

In the VOF model, the interface between the phases is tracked by solving a continuity equation for the volume fraction of one of the phases [36]. For the liquid phase, the continuity equation has the following form:

$$\frac{\partial(\rho_l \alpha_l)}{\partial t} + \nabla \cdot (\rho_l \alpha_l \mathbf{v}) = S_m \quad (9)$$

where  $\rho_l$  is the density of the liquid refrigerant,  $\text{kg}/\text{m}^3$ ;  $\mathbf{v}$  is the velocity of the heat pipe refrigerant,  $\text{m}/\text{s}$ ;  $t$  is the time,  $\text{s}$ ;  $S_m$  is the source term of mass,  $\text{kg}/\text{s}$ . It is assumed that the phase change occurs at the saturation temperature. The source term of mass  $S_m$  is calculated as follows:

$$S_{m,vl} = \begin{cases} \frac{r_{lv} \alpha_l \rho_l (T_l - T_{sat})}{T_{sat}} & T_l \geq T_{sat} \\ 0 & T_l < T_{sat} \end{cases} \quad (10)$$

$$S_{m,vl} = \begin{cases} \frac{r_{vl} \alpha_v \rho_v (T_{sat} - T_v)}{T_{sat}} & T_v \leq T_{sat} \\ 0 & T_v > T_{sat} \end{cases} \quad (11)$$

where  $S_{m,lv}$  is the mass source term for the conversion of the liquid phase into the vapor phase,  $S_{m,vl}$  is the mass source term for the conversion of the vapor phase into the liquid phase,  $\text{kg}/\text{s}$ ;  $T_{sat}$  is the saturation temperature,  $^\circ\text{C}$ ;  $T_l$  and  $T_v$  are the temperatures of the liquid and vapor phases, respectively,  $^\circ\text{C}$ ;  $r$  is the relaxation factor, dimensionless.

In the VOF model, the velocity field obtained from solving the momentum equation for a single phase is shared among the phases. The momentum equation is shown in Eq. (12).

$$\frac{\partial(\rho \mathbf{v})}{\partial t} + \nabla \cdot (\rho \mathbf{v} \mathbf{v}) = -\nabla p_h + \nabla \cdot [\mu (\nabla \mathbf{v} + \nabla \mathbf{v}^T)] + \rho \mathbf{g} + \mathbf{F}_s \quad (12)$$

In the case:

$$F_s = \sigma_{lv} \frac{\rho \kappa \nabla \alpha_l}{0.5(\rho_l + \rho_v)} \quad (13)$$

where  $p_h$  is the total pressure of the two phases in the heat pipe, Pa;  $F_s$  is the surface tension term,  $\text{N}/\text{m}^3$ ;  $\sigma_{lv}$  is the surface tension between the vapor and liquid phases,  $\text{N}/\text{m}$ ;  $\kappa$  is the surface curvature between the vapor and liquid phases, dimensionless.

The energy conservation equation in the VOF model is specified as:

$$\frac{\partial(\rho E)}{\partial t} + \nabla \cdot [\mathbf{v}(\rho E + p_h)] = \nabla \cdot (k \nabla T) + q_h \quad (14)$$

where  $E$  is the internal energy per unit mass of the vapor-liquid mixture and is further expressed by Eq. (15),  $J$ ;  $q_h$  is the energy source term caused by the phase change,  $\text{W}/\text{m}^3$ .

$$E = \frac{\alpha_v \rho_v E_v + \alpha_l \rho_l E_l}{\alpha_v \rho_v + \alpha_l \rho_l} \quad (15)$$

The phase change rate of the heat pipe refrigerant  $\dot{m}_h$  is expressed as Eq. (16); while  $q_h$  is given by Eq. (17) and (18), respectively.

$$\dot{m}_h = \frac{ha}{h_{fg}} \left[ \frac{\rho(T - T_{sat})}{\rho - \rho_l \alpha_l} \right] \quad (16)$$

$$q_h = ha \left[ \frac{\rho(T - T_{sat})}{\rho - \rho_l \alpha_l} \right] \quad (17)$$

$$q_h = \dot{m}_h h_{fg} \quad (18)$$

where  $h$  is the heat transfer coefficient,  $\text{W}/(\text{m}^2 \cdot ^\circ\text{C})$ ;  $a$  is the heat pipe area per unit volume,  $\text{m}^2$ ;  $h_{fg}$  is the latent heat, J.

## (3) Vapor compression sub-system.

The vapor compression sub-system consists mainly of an evaporator, a condenser, a compressor, and an electronic expansion valve (EEV). During the refrigerant circulation, the refrigerant flow rate and pressure distribution can be derived from the mass conservation equation:

$$\frac{d}{dt}(\rho_{vr} V) = \dot{m}_{vr,i} - \dot{m}_{vr,o} \quad (19)$$

where  $\rho_{vr}$  is the density of the refrigerant in the vapor compression subsystem,  $\text{kg/m}^3$ ;  $V$  is a control volume,  $\text{m}^3$ ;  $\dot{m}_{vr,i}$  is the mass flow rate into the control volume,  $\text{kg/s}$ ; and  $\dot{m}_{vr,o}$  is the mass flow rate out of the control volume,  $\text{kg/s}$ .

To consider the compressibility of the fluid, the fluid mass compression coefficient  $\lambda$  is introduced into Eq. (19) to obtain Eq. (20) [38].

$$\lambda \frac{dp_v}{dt} = \dot{m}_{vr,i} - \dot{m}_{vr,o} \quad (20)$$

where  $\lambda = \rho_{vr}V/\beta$  is the mass compression coefficient,  $\text{kg/Pa}$ ;  $\beta = \rho_{vr}dp_v/d\rho_{vr}$  is the bulk module of the fluid,  $\text{Pa}$ ;  $p_v$  is the pressure of the fluid in the vapor compression sub-system,  $\text{Pa}$ .

The compressor provides circulation power for the vapor compression loop. The refrigerant mass flow rate through the compressor is given by the following Eq. [39]:

$$m_{cr} = \eta_v \frac{V_c n_c}{60 v_c} \quad (21)$$

where  $\eta_v$  represents the volume efficiency of the compressor, %;  $V_c$  indicates the total volume of the compressor cylinder,  $\text{m}^3$ ;  $n_c$  is the rotation speed of the compressor,  $\text{r/min}$ ;  $v_c$  denotes the specific volume of the refrigerant at the compressor inlet,  $\text{m}^3/\text{kg}$ .

The mass flow rate of refrigerant through the EEV is calculated as [6]:

$$m_{er} = C_D K_e A_e \sqrt{2(p_{ei} - p_{eo})/v_{ei}} \quad (22)$$

where  $C_D$  is the flow coefficient, dimensionless;  $K_e$  indicates the opening of the EEV;  $A_e$  is the flow area,  $\text{m}^2$ ;  $p_{ei}$  and  $p_{eo}$  are the pressure at the inlet and outlet of the EEV, respectively,  $\text{Pa}$ ;  $v_{ei}$  is the refrigerant specific volume at the inlet of the EEV,  $\text{m}^3/\text{kg}$ .

In the evaporator and condenser, the refrigerant can be divided into superheated, two-phase, and subcooled zones [6]. In this case, the refrigerant is vapor in the superheated zone and liquid in the subcooled zone. The flow heat transfer equation between the refrigerant and the evaporator/ condenser tube wall can be expressed as:

$$\rho_{vr} C_{vr} \frac{dT_{vr}}{dt} = \dot{m}_{vr,i} h_{vr,i} - \dot{m}_{vr,o} h_{vr,o} = \alpha_{vr} (T_{vr,m} - T_w) \frac{dA_i}{dt} \quad (23)$$

where  $T_{vr}$  is the temperature of the refrigerant,  $^\circ\text{C}$ ;  $h_{vr,i}$  is the refrigerant enthalpy entering the control volume,  $\text{J/kg}$ ;  $h_{vr,o}$  is the refrigerant enthalpy leaving the control volume,  $\text{J/kg}$ ;  $\alpha_{vr}$  is the heat transfer coefficient of the refrigerant,  $\text{W}/(\text{m}^2 \cdot ^\circ\text{C})$ ;  $A_i$  is the heat transfer area of the tube per unit control volume,  $\text{m}^2$ ;  $T_w$  is the temperature of the tube wall,  $^\circ\text{C}$ ;  $T_{vr,m}$  is the mean temperature of the refrigerant,  $^\circ\text{C}$ .

The heat transfer coefficients of the refrigerant in the single-phase and two-phase zones are [40,41]:

$$\alpha_{vr,s} = \frac{\lambda_{vr} \cdot Nu_i}{d_i} \quad (24)$$

$$\alpha_{vr,d} = \alpha_{vr,s} \left[ (1 - \chi)^{0.8} + \frac{3.8\chi^{0.76}(1 - \chi)^{0.04}}{Pr^{0.38}} \right] \quad (25)$$

where  $Nu_i = 0.023Re^{0.8}Pr^{0.3}$ ,  $Re = m_{vr}d_i/\mu$ ,  $Pr = C_{vr}\mu/\lambda_{vr}$ ;  $\lambda_{vr}$  is the thermal conductivity of the refrigerant,  $\text{W}/(\text{m} \cdot ^\circ\text{C})$ ;  $m_{vr}$  is the mass flow density of the refrigerant,  $\text{kg}/(\text{m}^2 \cdot \text{s})$ ;  $d_i$  is the inner diameter of the evaporator/condenser tube,  $\text{m}$ ;  $\mu_{vr}$  is the dynamic viscosity of the refrigerant,  $\text{Pa}\cdot\text{s}$ ; and  $\chi$  is the dryness of the refrigerant, dimensionless.

In this study, K-Spice® [42], a dynamic process simulator developed by Kongsberg Digital Ltd., was used to solve the aforementioned governing equations (Eqs. (1)–(25)). First, the thermodynamics software Multiflash was used to calculate the physical and thermodynamic

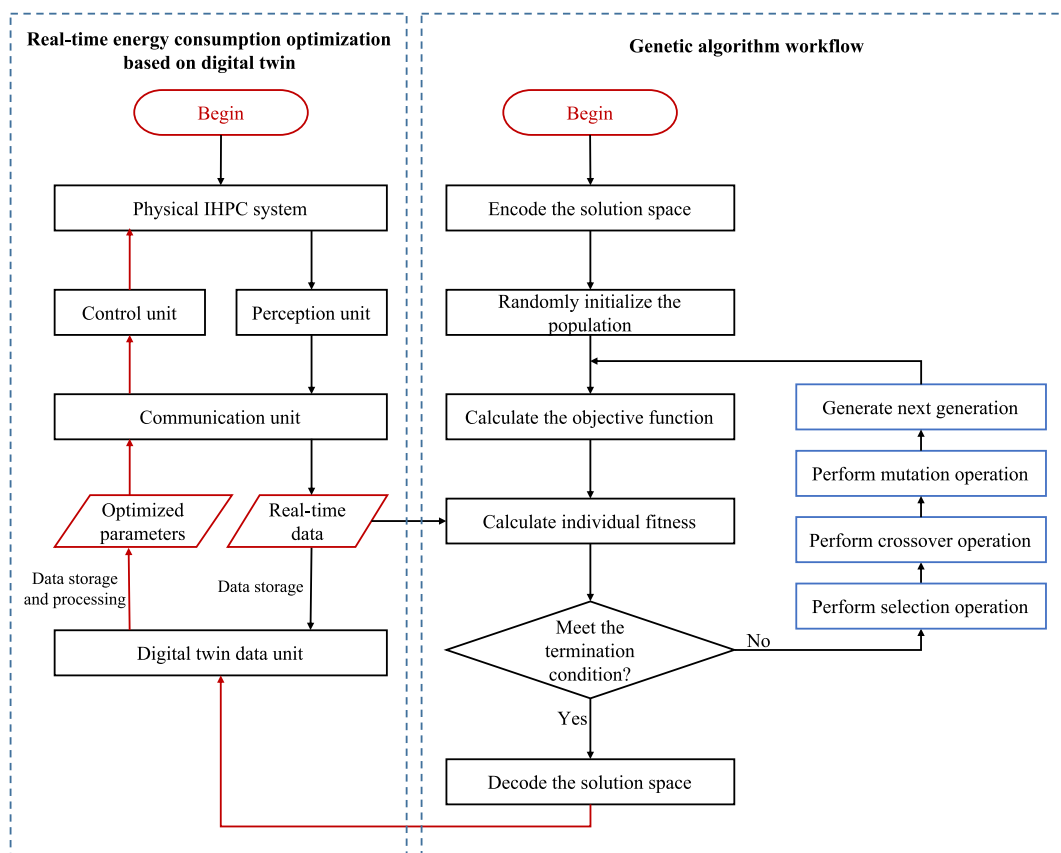
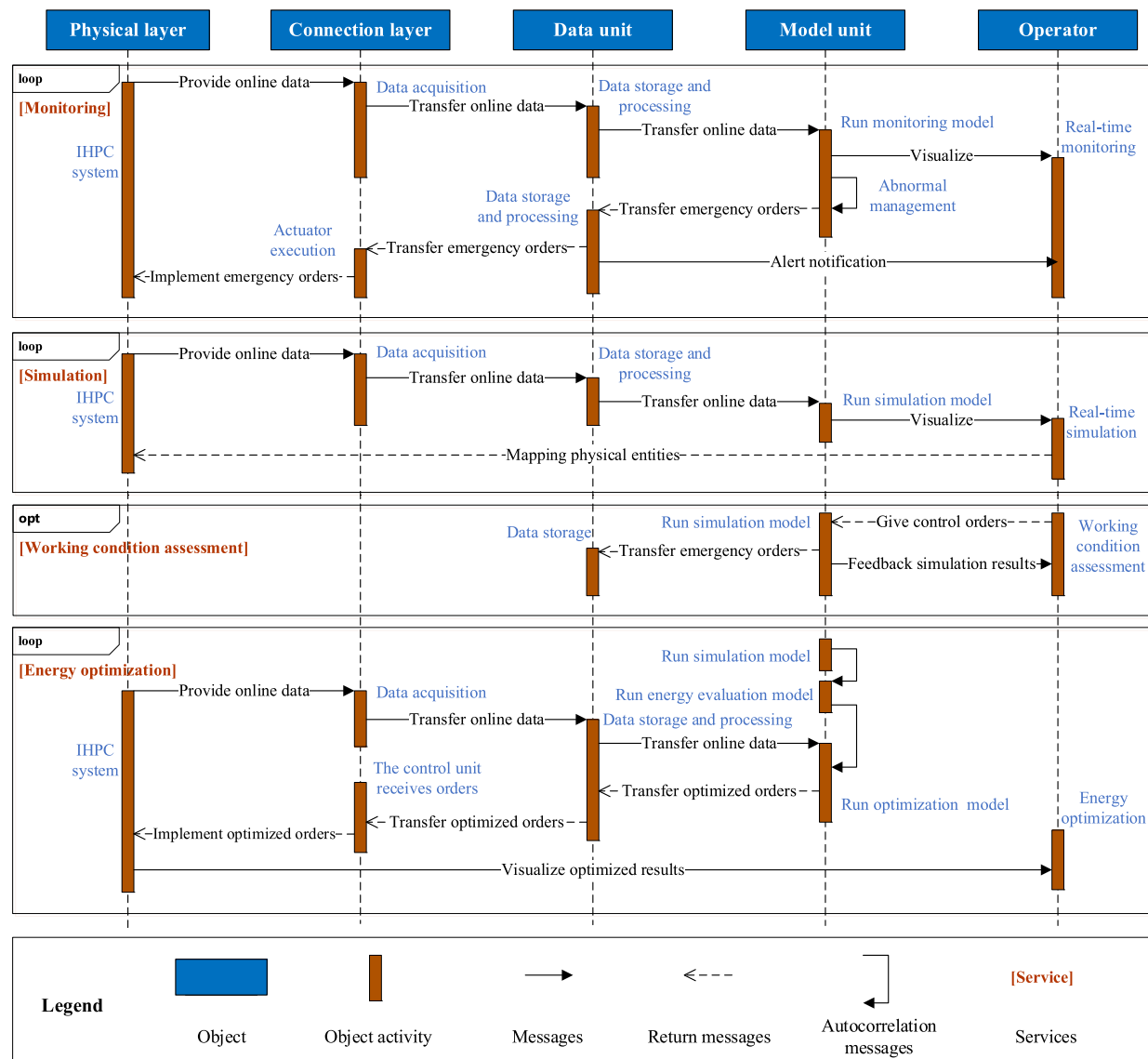


Fig. 4. Optimization process of the energy consumption based on the genetic algorithm.



**Fig. 5.** Interoperability among the layers in the digital twin architecture.

parameters of the refrigerant and generate the corresponding packages. Secondly, the generated thermodynamic packages were imported into K-Spice®, which was integrated with the components of the IHPC system. The empirical formulas (Eqs. (21), (22), (24), (25)) were employed by the corresponding components via user-defined functions. Finally, the K-Spice® software discretized these equations into a set of algebraic equations using the implicit Euler method and then solved the latter by applying the Newton-Raphson method [43].

#### 4.3. Energy evaluation and optimization model

##### 4.3.1. Energy evaluation model

In this section, an energy evaluation model is developed to predict and evaluate the total energy consumption of the IHPC system under various operating conditions. Two primary energy-consuming components exist in the IHPC system: the fan and the compressor. In this case, only the fans consume energy when the heat pipe sub-system works. The compressors will not consume energy until the vapor compression sub-system gets activated. Therefore, the total power consumption of an IHPC system is the sum of the power consumed by the fans and the compressors:

$$W_t = \sum_{i=1}^n W_{f,i} + \sum_{i=1}^m W_{c,i} \quad (26)$$

where  $W_t$ ,  $W_f$  and  $W_c$  are the power consumption of the IHPC system, the fan and the compressor, kW;  $n$  and  $m$  are the number of the running fans and the running compressors, respectively.

Typically, the power consumption of a fan can be evaluated by Eq. (27) [44].

$$W_f = kn_f^3 \quad (27)$$

where  $n_f$  is the speed of the fan, r/min;  $k$  is the performance parameter of the fan, dimensionless, which can be obtained by fitting the recorded operating data.

The power consumption of a compressor can be described as Eq. (28) [6].

$$W_c = m_r \frac{h_s - h_{in}}{\eta_c \eta_s} \quad (28)$$

where  $h_{in}$  is the enthalpy of the refrigerant at the compressor inlet, J/kg;  $h_s$  denotes the enthalpy of the refrigerant at the compressor outlet, J/kg;

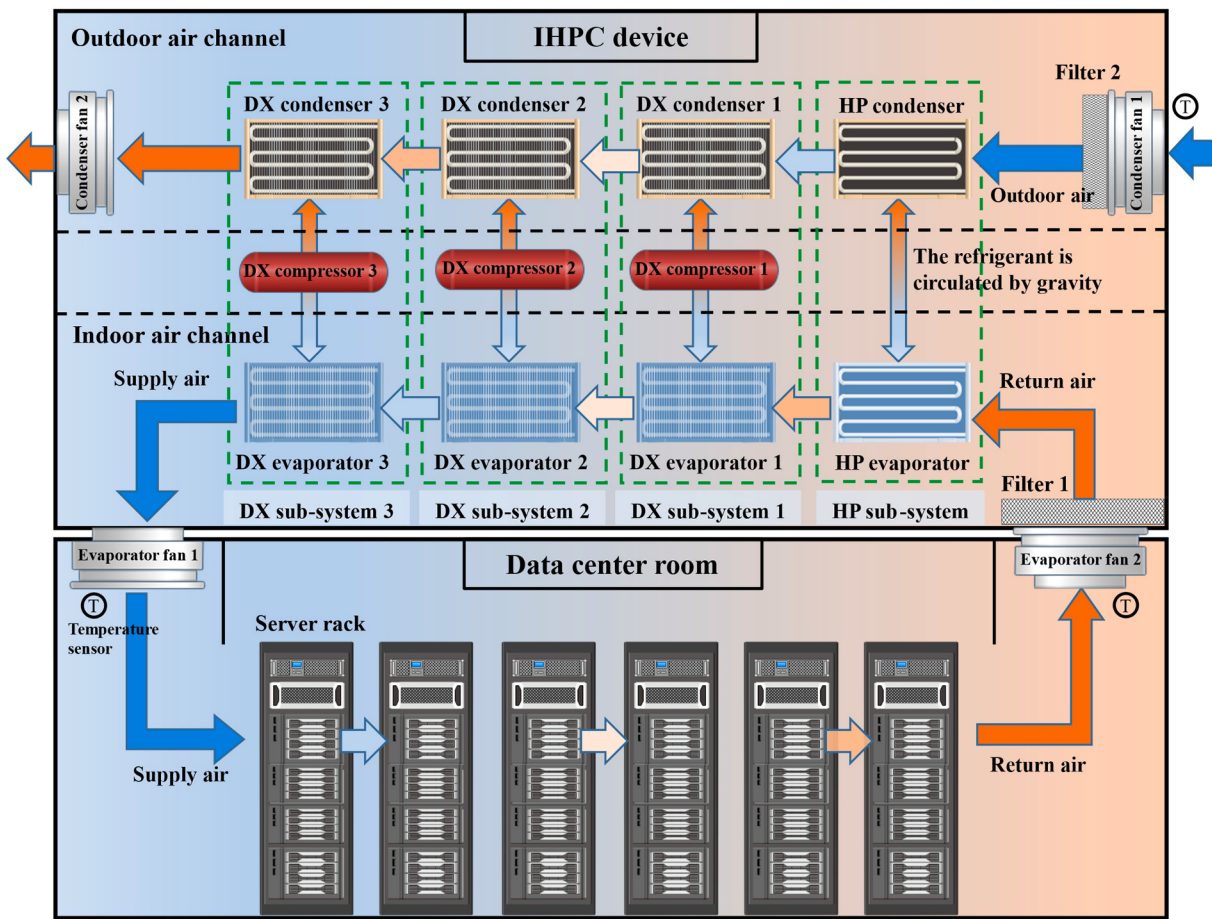


Fig. 6. Diagram of the air circulation via the IHPC system in the data center room.

$\eta_c$  is the heat loss coefficient of the compressor, %;  $\eta_s$  is the isentropic efficiency of the compressor, %.

The total energy consumption of the IHPC system is:

$$E_{\text{cool}} = \sum_{i=1}^n W_{f,i} t_{f,i} + \sum_{i=1}^m W_{c,i} t_{c,i} \quad (29)$$

where  $E_{\text{cool}}$  indicates the total energy consumption of the IHPC system, kWh;  $t_f$  and  $t_c$  are the working time of the fan and compressor, respectively, h.

The unknown coefficients in Eqs. (27)–(28) were obtained by fitting the historically operational data of the IHPC system. Such a fitting problem was solved by using the Levenberg-Marquardt algorithm to obtain the coefficients [45,46]. The fitting performance is evaluated by the coefficient of determination  $R^2$ :

$$R^2 = 1 - \frac{\sum_{i=1}^n (y_i - \hat{y}_i)^2}{\sum_{i=1}^n (y_i - \bar{y})^2} \quad (30)$$

where  $y_i$  is the energy consumption from the  $i$ th measurement;  $\hat{y}_i$  is the energy consumption from the  $i$ th prediction;  $n$  is the total number of measurements and predictions;  $\bar{y}$  is the averaged energy consumption from measurement.

Moreover, the overall performance of the IHPC system is evaluated by using the coefficient of performance (COP) [6]:

$$\text{COP} = \frac{Q_{\text{cool}}}{W_t} = \frac{Q_{\text{cool}}}{\sum_{i=1}^n W_{f,i} + \sum_{i=1}^m W_{c,i}} \quad (31)$$

where  $Q_{\text{cool}}$  is the total cooling capacity of the IHPC system, kW;  $W_t$  is the total power consumption of the IHPC system, kW.

The PUE is employed to assess the overall energy efficiency of a data center [2]:

$$\text{PUE} = \frac{E_{\text{data}}}{E_{\text{IT}}} = \frac{E_{\text{IT}} + E_{\text{cool}} + E_{\text{light}}}{E_{\text{IT}}} \quad (32)$$

where  $E_{\text{data}}$  is the total energy consumption of the data center, kWh;  $E_{\text{IT}}$  is the energy consumption of the IT (information technology) equipment, kWh;  $E_{\text{light}}$  is the energy consumption of the lighting equipment, kWh.

#### 4.3.2. Energy optimization model

The objective of energy optimization is to optimize the operating conditions so that the cooling requirements and the IHPC system health are ensured while the energy consumption gets minimized. In this research, the genetic algorithm is employed to solve the energy optimization model, which is defined as:

$$\min E_{\text{cool}}(n_{f,c}, n_{f,e}, n_c) \quad (33)$$

s.t.

$$\begin{cases} T_s \leq T_{s,\text{threshold}} \\ T_r \leq T_{r,\text{threshold}} \end{cases} \quad (34)$$

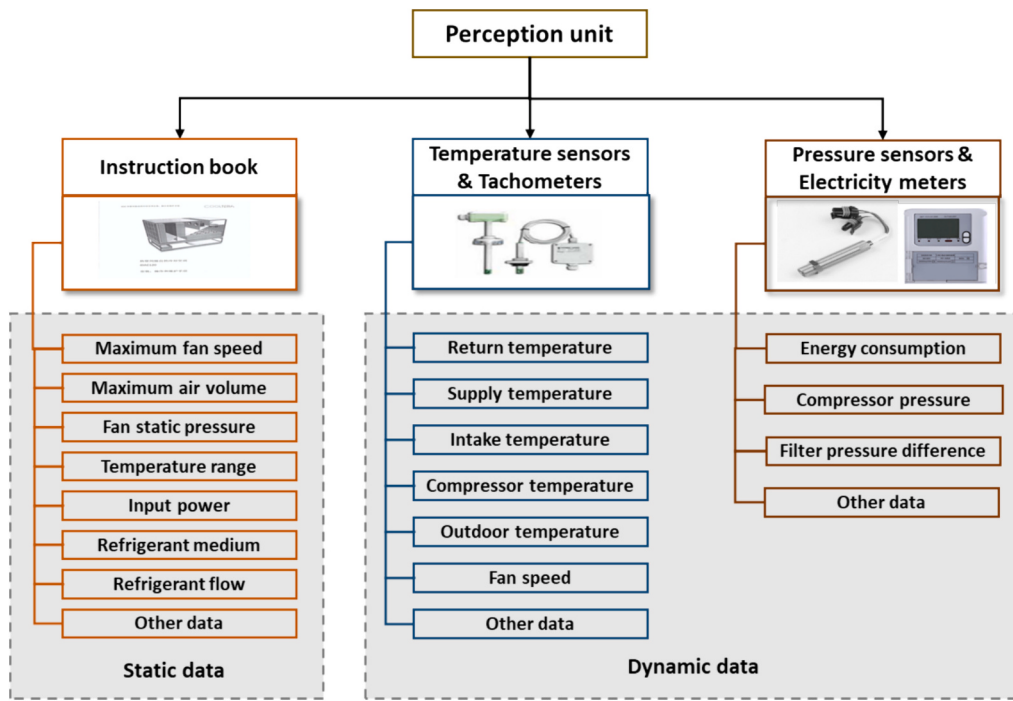


Fig. 7. Digital twin perception unit and the perception tools.

where  $n_{f,c}$ ,  $n_{f,e}$  and  $n_c$  are the rotation speed of the condenser fan, the evaporator fan, and the compressor, r/min;  $T_s$  is the supply air temperature, °C;  $T_{s,\text{threshold}}$  is the threshold for the supply air temperature, °C;  $T_r$  is the return air temperature, °C;  $T_{r,\text{threshold}}$  is the threshold for the return air temperature, °C. The derivation of  $T_{s,\text{threshold}}$  and  $T_{r,\text{threshold}}$  is presented in Appendix A.

The solution space is restricted to the corresponding value ranges of the aforementioned  $n_{f,c}$ ,  $n_{f,e}$  and  $n_c$  to keep the IHPC system healthy. In addition, to satisfy the constraints given in Eq. (34) the fitness function of the individual is defined as:

$$e = \Delta - E_{\text{cool}} - \lambda_1 P_1(T_s) - \lambda_2 P_2(T_r) \quad (35)$$

where  $e$  is the individual fitness, dimensionless;  $\Delta$  is the total energy consumption of the IHPC system at its maximum load, kWh;  $P_1(T_s)$  and  $P_2(T_r)$  are the penalty functions used to satisfy the constraints (Eq. (34)),

which are  $P_1(T_s) = \max(0, T_s - T_{s,\text{threshold}})$  and  $P_2(T_r) = \max(0, T_r - T_{r,\text{threshold}})$ ;  $\lambda_1$  and  $\lambda_2$  are the penalty coefficients for the penalty functions  $P_1(T_s)$  and  $P_2(T_r)$ , respectively.

The energy optimization process based on the genetic algorithm is shown in Fig. 4.

#### 4.4. Interoperability between layers in the digital twin architecture

The internal components of the digital twin communicate and collaborate with each other during its service life. This section describes the mechanism of interaction and collaboration between digital twin components when delivering services, as shown in Fig. 5.

In the monitoring service, the real-time data generated in the physical layer are captured by the perception unit in the connection layer and transferred to the data unit in the digital layer for storage and

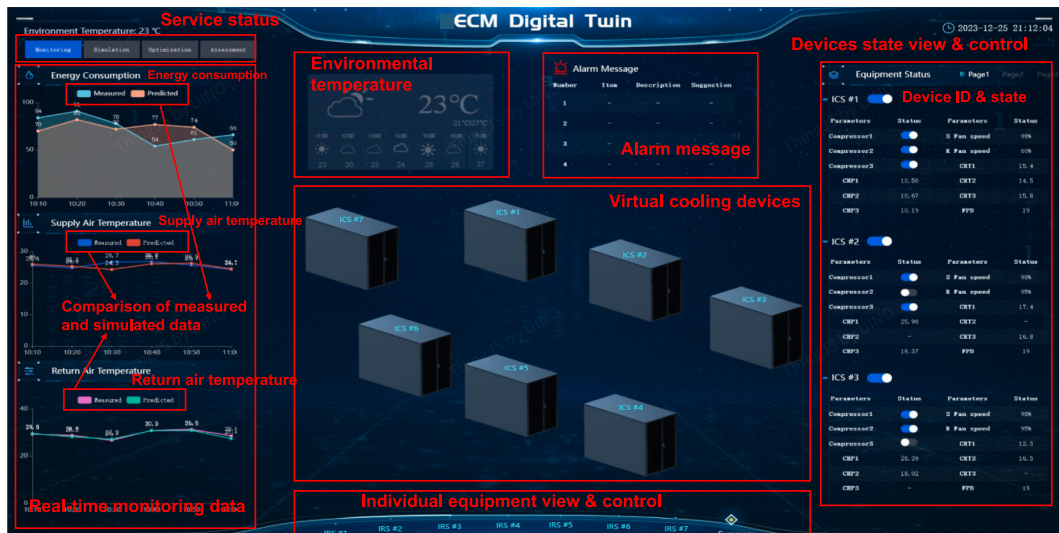


Fig. 8. Interactive interface of the ECM digital twin.



Fig. 9. Operational status view and control interface of the individual devices.

processing. The real-time data is then transferred to the model unit where the monitoring model is activated. The captured data and the orders output from the monitoring model are saved and visualized. An alert notification is displayed to the operator when an abnormality is

detected. In the simulation service, the real-time data are transferred to the model unit, followed by the activation of the simulation model to realize the real-time mapping of the physical entity, from which the simulation results are presented to the operator instantaneously. The

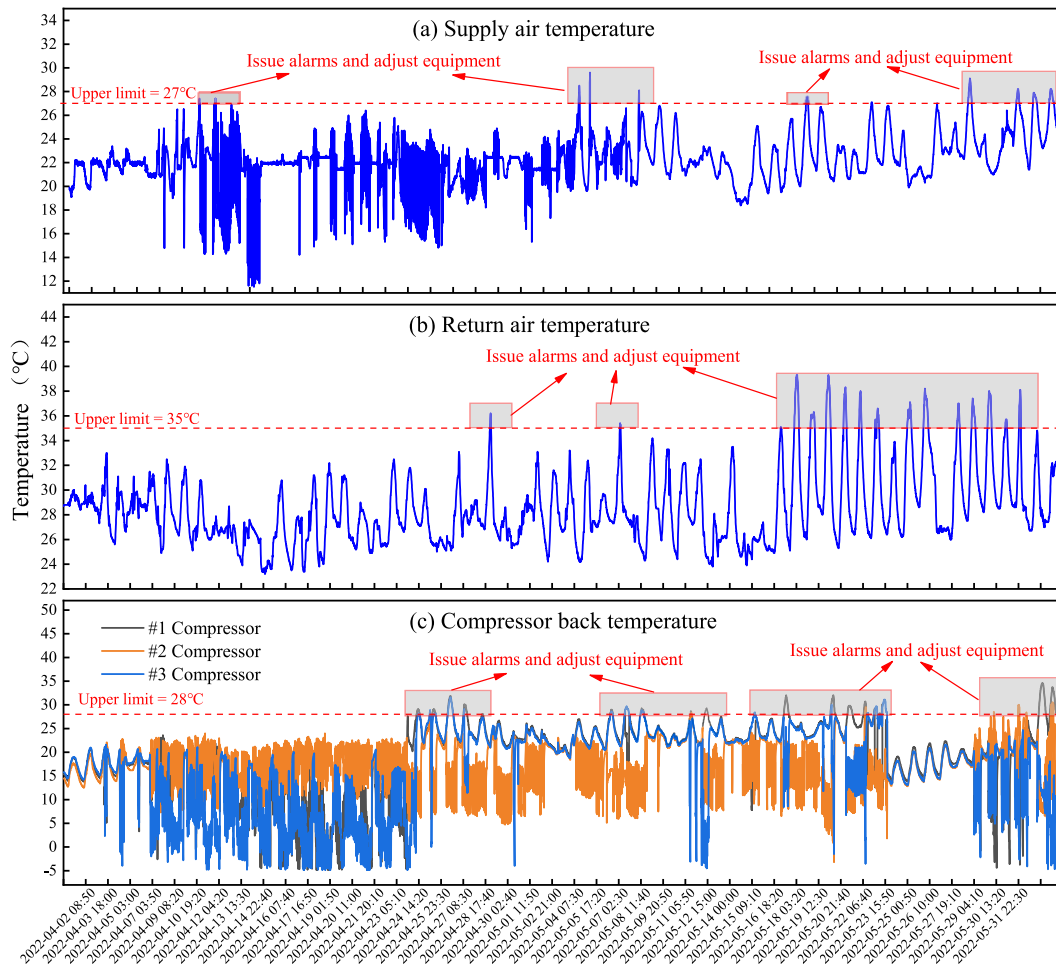
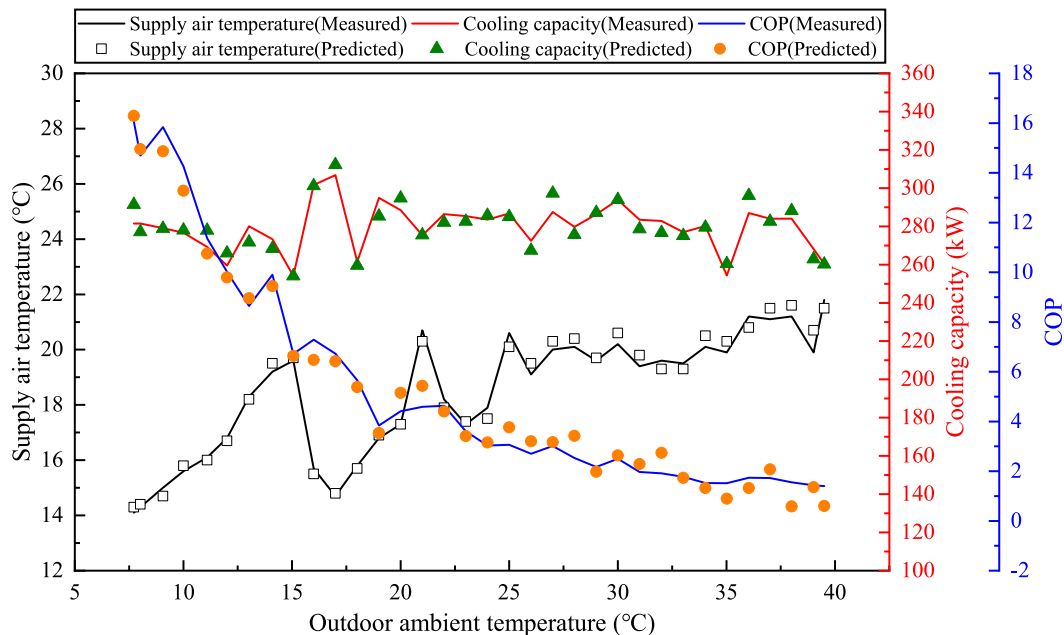


Fig. 10. Real-time abnormality detection and automatic adjustment of the key parameters.



**Fig. 11.** Comparison of the digital twin predicted values against the measured data.

operator must input the operating parameters of the IHPC system into the working condition assessment service. These parameters include the outdoor temperature, return air temperature, fan speed, and number of compressors activated. After the simulation model is activated, the digital twin provides the operator with a virtual space to assess the effects of the operating parameters on the physical entity. In the energy optimization service, the energy evaluation model, the simulation model, and the energy optimization model are activated simultaneously. The optimized orders are then transferred to the controller in the connection layer for implementation in a real system.

## 5. Case study

### 5.1. Background

An IHPC system typically consists of multiple cooling devices. In this case, an IHPC system consisting seven IHPC devices was deployed in parallel on the top of a data center room in Shanghai, China. The internal structure and air circulation flow of one of the devices and a row of server racks inside the data center room are displayed in Fig. 6. The cold air enters the data center via the evaporator fan 1, where it is distributed to each server rack through the air supply channel and mixed with the hot air surrounding the server racks. Such a process decreases the average temperature of the data center room. The mixed, heated air passes through the indoor air channel of the IHPC device via the evaporator fan 2 and then returns to the data center after being cooled by the evaporators. Simultaneously, the outdoor cold air ventilates along the outdoor air channel of the device, where it indirectly exchanges heat with the warm air inside the indoor air channel.

As shown in Fig. 6, the IHPC device in this case contains a heat pipe (HP) sub-system and three direct expansion (DX) sub-systems (a type of vapor compression system). The HP sub-system that provides free cooling consists of an HP evaporator and an HP condenser. In this case, the HP condenser and HP evaporator are L-shaped heat pipes in which the refrigerant is circulated by gravity. The DX sub-system mainly consists of a DX evaporator, a DX condenser and a compressor, which is employed to provide mechanical refrigeration. The refrigerant medium used in the HP sub-system is R134a, while the refrigerant medium inside the DX sub-system is R410a. The maximum cooling capacity and maximum input power of an IHPC device is 120.0 and 50.6 kW,

respectively. The input power of each evaporator fan, condenser fan, and compressor is 3.5, 5.5, and 10.9 kW, respectively. Meanwhile, the manufacturer specifies that the heat exchange efficiency of the heat pipe is no <65%. The IHPC system preferentially cools the return air using the HP sub-system (free cooling), given that the HP sub-system works at a lower power than the DX sub-system. When the HP sub-system is unable to maintain the cooling level, the compressors are sequentially turned on to activate the DX sub-system (mechanical refrigeration).

### 5.2. Connection layer and visualization deployment

This section describes the units in the architectural connection layer, as well as the visualization that improves the efficiency of human-computer interaction.

In this study, the devices within the IHPC system were connected to each other by twisted pair wires using the Controller Area Network-BUS (CANBUS) as the communication protocol. The IHPC system was linked to the external computer through the wired transmission using the Modbus protocol and the RS-485 physical interface. The Application Programming Interfaces (APIs) were used to transmit data among various units within the digital twin.

The perception unit of the IHPC system is displayed in Fig. 7. The primary tools for obtaining data in the perception unit include the instruction manual, temperature sensors, pressure sensors, tachometers, and electricity meters. The parameters obtained from the instruction manual are static design parameters such as the maximum speed of the fan, maximum airflow, static pressure, and input power. The dynamic data were those acquired from sensors, tachometers, and electricity meters, including the supply air temperature, return air temperature, fan speed, and power consumption during the operation of the equipment.

In this study, a Programmable Logic Controller (PLC) was applied to control the physical system. The control parameters include the condenser fan speed, evaporator fan speed, and device status.

It is imperative to visualize the IHPC system in a digital space to facilitate the interaction between the digital twin and the human for the efficient system management. The digital twin for the IHPC system was developed and demonstrated using the JavaScript programming language and Vue.js framework, as shown in Fig. 8. The lower center of Fig. 8 displays seven virtual cooling devices, while the left and right parts display the real-time health monitoring data of the physical ones.

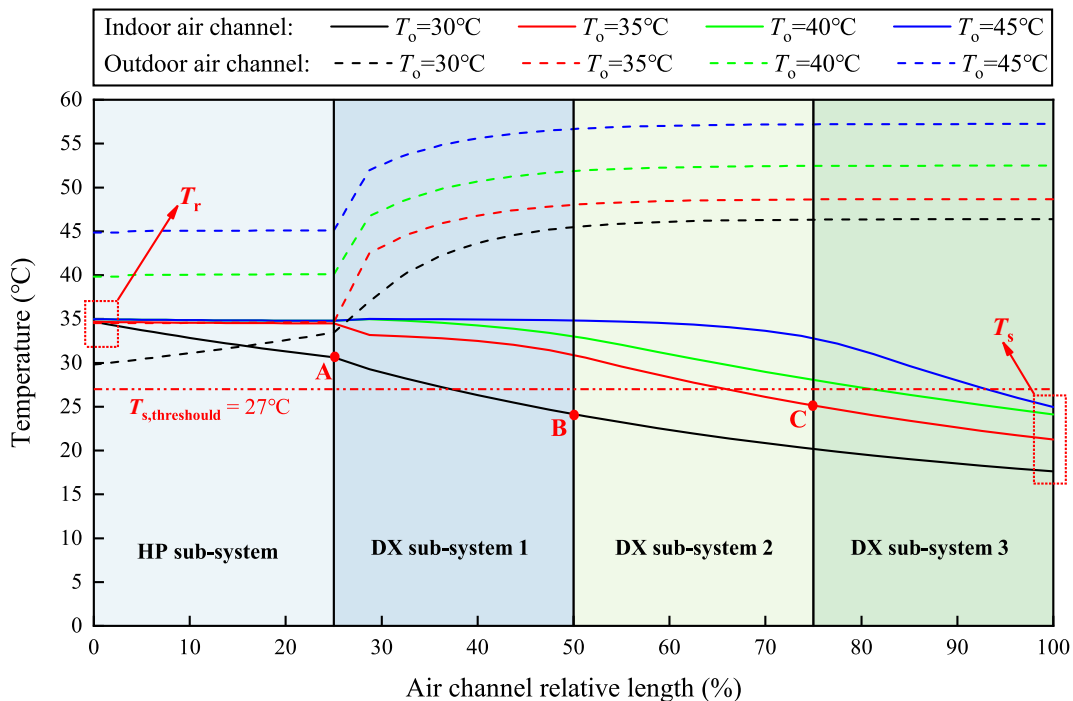


**Fig. 12.** Assessment on the IHPC system working condition at different outdoor temperatures.

The perception unit collected all the real-time data from the IHPC system to feed to the monitoring service, as demonstrated by the “Real-time monitoring data” panel in Fig. 8. For situations that may endanger the health of a physical device, the digital twin issues and displays the alarm information in the “Alarm message” panel. Meanwhile, the predicted results of the simulation model are displayed and compared with the real-time data. The outdoor temperature obtained through the API is displayed online on the “Environmental temperature” panel. Compared with the “Summary” panel, the “Individual equipment view and control” panel presents the immediate monitoring data of an individual device as well as the operating status of the device, as shown in Fig. 9. Finally, the digital twin provides an interface for the interaction with the operators, who can view and adjust the operating parameters of the physical device directly on the digital twin (by using the “Devices state view & control” panel).

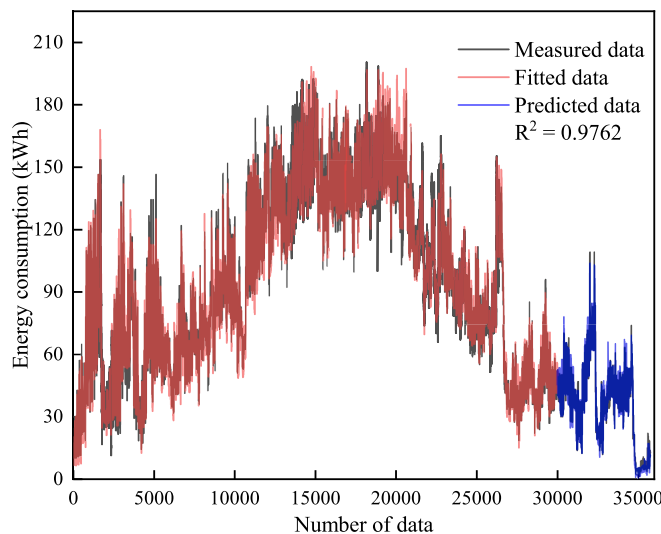
In a digital twin system, the real-time interaction between the digital twin model and the sensors ensures the accuracy of the model and its synchronization with the physical entity. However, the incompatibility between the data acquisition and the system response speed remains a significant challenge. The following strategies are adopted in this research to tackle such a challenge. First, the developed ECM digital twin was deployed on the industrial computer inside the data center to reduce the impact of network fluctuation on the system stability. Secondly, the wired transmission method was used for the data transmission to avoid potential interference and to improve the speed as well as the stability of the data flow. Finally, a synchronization rate among the data acquisition, transmission, and system response was implemented at a time interval of 10 min, ensuring that the physical entity and the ECM digital twin were synchronized at an acceptable speed.

### 5.3. Results and discussion

In the monitoring service, the parametric thresholds and real-time operating data of the IHPC system are fed into the monitoring model, which carries out real-time monitoring, abnormality assessment, and automatic adjustment of the IHPC system. The real-time abnormality detection and automatic adjustment results of the key parameters are displayed in Fig. 10. The upper temperature limits for the supply air,

return air, and compressor are 27, 35, and 28 °C, respectively. These threshold data were collected from both the cooling requirements of the data center and the technical specifications on the manufacturer manual. The health of the IHPC system cannot be guaranteed when the recorded data exceed their upper limits. On the contrary, the digital twin can be triggered to capture the abnormal signals, issue the appropriate alarms, and adjust the operating parameters of the physical equipment. When the temperature of the supply air or return air exceeds the threshold, the digital twin issues an alarm (shown in the “Alarm message” panel in Fig. 8) based on Algorithm 2 and automatically adjusts the status of the fans, compressors, and standby IHPC devices to gradually increase the cooling capacity until the temperature falls below the threshold. When the pressure and back temperature of a compressor exceed the upper limit values set by the manufacturer, overload and damage may occur to the compressor. In this circumstance, the digital twin first issues an alarm message (as shown in the “Alarm message” panel in Fig. 8) to notify the device administrator, then turns off the abnormal compressor and activates a vacant compressor to replace the former compressor. The abnormal compressor will be inactive until its measured temperature falls within the normal range. These alarms will be stored in the database after notifying the administrator. The stored alarm information also provides data to feed into the optimization work on the equipment management. Moreover, the digital twin can handle the uncertainties during the operation of the data center. As shown in Fig. 10(b), the return air temperature frequently exceeds its upper limit at the later stage because of the sudden increase in heat output of the IT equipment. After the digital twin deployment, the return air temperature can quickly drop below the warning line.

When the predicted values do not match the actual ones (e.g., the supply air temperature values in Figs. 8 and 9), the anomaly management process follows: First, it is necessary to determine whether the measured value exceeds its upper limit. If not (Fig. 8), the equipment and system health can be assured. In this case, the deviation between the predicted and measured values needs to be evaluated. The digital twin model will be calibrated by checking and synchronizing the consistency of the working state between the digital twin model and the real cooling system when the deviation becomes unacceptable. Next, when the measured value rises beyond its limit (e.g., the supply air temperature in



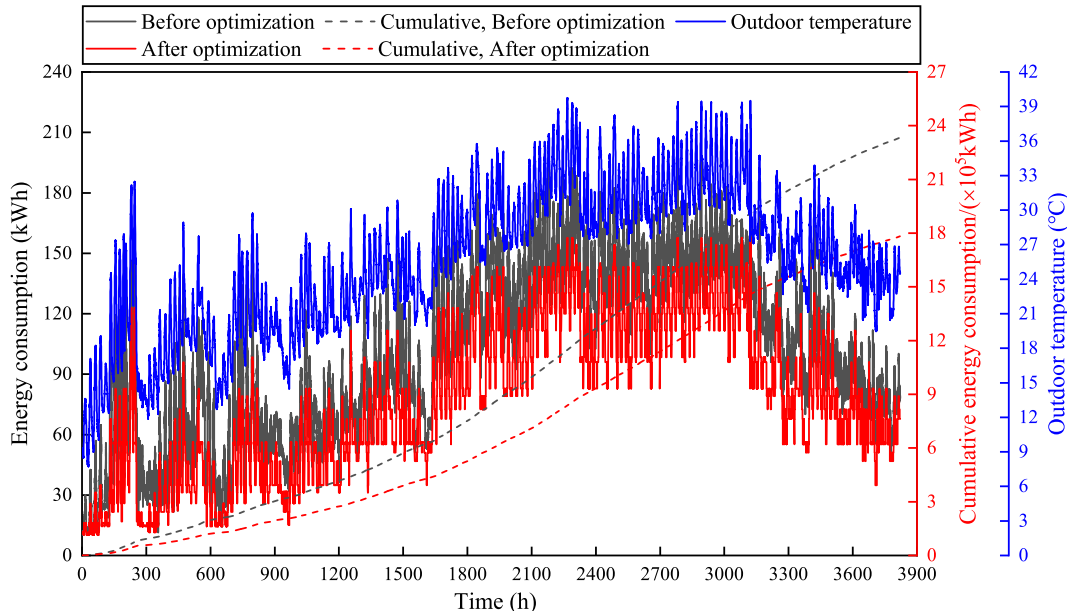
**Fig. 13.** Fitting and validation results of the energy evaluation model.

Fig. 9), the abnormal condition will be handled by Algorithm 2 in the monitoring model (Always-on). The handling result is shown in Fig. 9, where the value of the supply air temperature ( $26.8^{\circ}\text{C}$ ) drops below its upper limit at the next measurement round.

In the simulation service, the digital twin maps the physical entity by real-time simulation to achieve the synchronization between the physical entity and the digital twin. The accuracy of the simulation model directly impacts the degree of synchronization between the digital twins and the physical system. The accuracy of the simulation model was validated by comparing the predicted values against the measured data, as is displayed in Fig. 11. In this case, the compressors remained inactive until the outdoor ambient temperature exceeded  $19^{\circ}\text{C}$ . The validation results indicate that the mean relative deviation of the cooling capacity is 1.46% and that for the supply air temperature is 1.43%. The COP records a mean relative deviation of 8.44% and decreases with an increase in the outdoor ambient temperature. The validation accuracies can satisfy the allowable engineering errors, thereby ensuring the synchronization between the digital twin and the physical system. Moreover, the discovered COP trends are consistent with the experimental

findings of He et al. [5]. The phenomenon is mainly attributed to the fact that the power consumption of the IHPC system increases with the growth of the outdoor temperature at a constant cooling capacity. When the free cooling model is exclusively employed (as the outdoor ambient temperature is  $5\text{--}19^{\circ}\text{C}$ ), only the HP sub-system works independently, the fans are the primary energy-consuming devices of the IHPC system. The cooling capacity of the IHPC system gradually decreases as the outdoor temperature rises. Therefore, the fan speed must be increased to improve the heat exchange rate and prevent this decline. According to Eq. (27), the increase in the fan speed will result in a significant increase in power consumption, leading to a sharp drop in COP. Meanwhile, as the outdoor ambient temperature rises, the condensing temperature of the vapor compression sub-system increases, resulting in a declined cooling capacity of the IHPC system. As a result, more compressors were activated to maintain the cooling capacity, which lead to an increasing power consumption of the IHPC system and a decreasing COP.

The working condition assessment service is driven by the simulation model. The operator assesses the working condition of the physical system in the virtual space by setting the different combinations of parameters. The temperature profiles of the indoor and outdoor air channels in the IHPC device are shown in Fig. 12, covering the outdoor temperature  $T_o$  over 30, 35, 40, and  $45^{\circ}\text{C}$ . In this case, the HP sub-system and the three DX sub-systems are deployed sequentially and turned in the air channels and all turned on, as shown in Fig. 6 and Fig. 12. The return air temperature is set at its upper limit of  $35^{\circ}\text{C}$ . The HP sub-system in Fig. 12 shows that the heat pipe works only when the outdoor temperature is lower than the return air temperature. The system is able to reduce the return air temperature from  $35.0^{\circ}\text{C}$  to  $30.6^{\circ}\text{C}$  via the free cooling model at an outdoor temperature of  $30^{\circ}\text{C}$  (point A in the “HP sub-system” zone of Fig. 12). In addition, the assessment results show that for  $T_o$  lower than  $45^{\circ}\text{C}$ ,  $T_r$  is cooled to below  $27^{\circ}\text{C}$  (“ $T_s$ ” in Fig. 12) by activating all the three DX sub-systems to meet the cooling needs. From an energy-saving perspective, the DX sub-systems should be activated gradually to increase the cooling capacity as the outdoor temperature rises. For instance, the DX sub-system 1 needs to be activated to meet the cooling demand when the  $T_o$  is  $30^{\circ}\text{C}$  (point B in Fig. 12), whereas the DX sub-system 2 also has to be triggered when the  $T_o$  rises up to  $35^{\circ}\text{C}$  (point C in Fig. 12). Meanwhile, the cooling capacity of the IHPC system gradually drops with an increase of  $T_o$  under the same operating parameters, which eventually leads to the decrease of COP. Such a phenomenon is mainly caused by the increased condensing



**Fig. 14.** Optimization on the energy consumption of the IHPC system after applying the digital twin.

temperature and the compressor energy consumption with an increase of  $T_o$ . In general, the working condition assessments can verify the stability and reliability of the physical system, and further provide data support for the design optimization of the physical system.

The energy optimization service is driven by the simulation, energy evaluation and optimization models. The specific data and workflow among the models are demonstrated in Fig. 5. In order to obtain the unknown coefficients in the energy evaluation model (Eqs. (27)–(28)), 30,000 energy consumption data points obtained from the electric meters were used for the fitting, and an additional 5900 data points were used for validation. Fig. 13 shows that the fitted values are in good agreement with the actual measured at an  $R^2$  of 0.9762 and an RMSE of merely 0.5 kWh.

The actual operating data of the IHPC system recorded by the sensors were fed into the energy optimization model to optimize the system energy consumption in real-time. The time interval of the optimization model was prescribed to be 10 min to match the actual recording frequency. Fig. 14 demonstrates that the energy consumption of the system reduces after optimization with the fulfilled cooling requirements. After the implementation of the digital twin, the cumulative energy consumption decreased from  $23.3390 \times 10^5$  kWh to  $17.8229 \times 10^5$  kWh. A total energy volume of  $5.5161 \times 10^5$  kWh had been saved after optimizing the system operating parameters, comprising 23.63% of the entire energy consumption. Furthermore, the average PUE of the data center reduced from 1.325 to 1.248 after optimizing the energy consumption of the IHPC system.

## 6. Conclusions and future work

This study proposes a digital twin approach for an efficient and automated ECM of the IHPC system. The feasibility and effectiveness of this digital twin approach were verified through a case study on the cooling system of a data center. Several conclusions can be drawn as follows.

Compared with the conventional methods, the proposed digital twin approach can automatically capture the abnormal conditions of the IHPC system in real-time. Meanwhile, the working states of the system were dynamically adjusted through the communication and control units to maintain the system health. In addition, benefiting from its perception unit, the digital twin can capture the online field data and dynamically simulate its working processes. The validation results show that the mean relative error between the digital twin simulated and the on-site measured supply air temperature is 1.43% and that for the

cooling capacity is 1.46%. The power consumption after a half-year run had been reduced by 23.63%, while the health of the equipment was assured and the cooling needs were satisfied ( $T_s \leq 27^\circ\text{C}$  &  $T_r \leq 35^\circ\text{C}$ ). The findings demonstrate the feasibility and practicability of the digital twin approach.

The digital twin approach provides a viable route for practitioners to tackle similar energy management projects. Future work can be dedicated to the following three areas of study. First, the data-driven AI models can be integrated to improve the self-awareness, self-learning, and self-decision capability of the digital twin. Secondly, although the digital twin of this study was built based on the existing hardware facilities, integration with other enterprise systems such as MES (Manufacturing Execution System), PMS (Production Management System), and ERP (Enterprise Resource Planning) is desired, so as to take full advantage of the digital twin. Last but not least, it is also necessary to integrate the proposed digital twin with the one for the data center via the reserved interfaces such that more valuable decisions for the management of the data center become possible.

## CRediT authorship contribution statement

**Haitao Zhu:** Writing – review & editing, Writing – original draft, Software, Methodology, Investigation. **Botao Lin:** Writing – review & editing, Writing – original draft, Project administration, Funding acquisition.

## Declaration of competing interest

The authors declare that they have no known competing financial interests or personal relationships that could have appeared to influence the work reported in this paper.

## Data availability

The data that has been used is confidential.

## Acknowledgment

We sincerely appreciate the funding provided by the National Natural Science Foundation of China (No.42277122). We would also like to express our gratitude towards the mentioned data center in Shanghai city for providing us with the operating data of its cooling system.

## Appendix A. Derivation of supply and return air temperature thresholds

The heat loss from the walls of the data center room is ignored. For the health of the IT equipment inside the data center, Eq. (A1) must be satisfied.

$$\dot{Q}_{IT,max} \leq \dot{Q}_{cool,max} \quad (A1)$$

In this case:

$$\dot{Q}_{IT,max} \leq C_a \dot{m}_{a,max} (T_r - T_s) \quad (A2)$$

where  $\dot{Q}_{IT,max}$  is the maximum heat generation rate of the IT equipment, J/s;  $\dot{Q}_{cool,max}$  indicates the maximum heat transfer rate of the cooling system, J/s;  $C_a$  is the specific heat capacity of the air, J/(kg·°C);  $\dot{m}_{a,max}$  is the maximum mass flow rate of the air, kg/s. The values of  $\dot{Q}_{IT,max}$  and  $\dot{m}_{a,max}$  can be obtained when the IT equipment and the cooling system are specified. Subsequently, the temperature difference between supply and return air can also be determined:

$$\frac{\dot{Q}_{IT,max}}{C_a \dot{m}_{a,max}} \leq (T_r - T_s) \quad (A3)$$

Therefore, the temperature thresholds of the supply and return air can be determined:

$$\begin{cases} T_r \leq T_{r,\text{threshold}} = T_{\text{IT,tolerance}} \\ T_s \leq T_{s,\text{threshold}} = T_{\text{IT,tolerance}} - \frac{\dot{Q}_{\text{IT,max}}}{C_a \dot{m}_{a,\text{max}}} \end{cases} \quad (\text{A4})$$

where  $T_{\text{IT,tolerance}}$  is the maximum temperature that an IT equipment can tolerate, °C.

## References

- [1] Dai J, Das D, Ohadi M, Pecht M. Reliability risk mitigation of free air cooling through prognostics and health management. *Appl Energy* 2013;111:104–12. <https://doi.org/10.1016/j.apenergy.2013.04.047>.
- [2] He W, Zhang J, Li H, Liu S, Wang Y, Lv B, et al. Optimal thermal management of server cooling system based cooling tower under different ambient temperatures. *Appl Therm Eng* 2022;207:118176. <https://doi.org/10.1016/j.aplthermaleng.2022.118176>.
- [3] Yu H, Zhang T, Chen L, Tao W. Refrigeration equipment model construction based in data center cooling station. *Int J Green Energy* 2023;1–9. <https://doi.org/10.1080/15435075.2023.2194374>.
- [4] He W, Ding S, Zhang J, Pei C, Zhang Z, Wang Y, et al. Performance optimization of server water cooling system based on minimum energy consumption analysis. *Appl Energy* 2021;303:117620. <https://doi.org/10.1016/j.apenergy.2021.117620>.
- [5] He Z, Xi H, Ding T, Wang J, Li Z. Energy efficiency optimization of an integrated heat pipe cooling system in data center based on genetic algorithm. *Appl Therm Eng* 2021;182:115800. <https://doi.org/10.1016/j.aplthermaleng.2020.115800>.
- [6] Han Z, Sun X, Wei H, Ji Q, Xue D. Energy saving analysis of evaporative cooling composite air conditioning system for data centers. *Appl Therm Eng* 2021;186:116506. <https://doi.org/10.1016/j.aplthermaleng.2020.116506>.
- [7] Wang Z, Zhang X, Li Z, Luo M. Analysis on energy efficiency of an integrated heat pipe system in data centers. *Appl Therm Eng* 2015;90:937–44. <https://doi.org/10.1016/j.aplthermaleng.2015.07.078>.
- [8] Wang X, Wen Q, Yang J, Xiang J, Wang Z, Weng C, et al. A review on data Centre cooling system using heat pipe technology. *Sustainable Comput-Infor* 2022;35:100774. <https://doi.org/10.1016/j.suscom.2022.100774>.
- [9] Kritzinger W, Karner M, Traar G, Henjes J, Sihm W. Digital twin in manufacturing: a categorical literature review and classification. *IFAC-PapersOnline*. 2018;51(11):1016–22. <https://doi.org/10.1016/j.ifacol.2018.08.474>.
- [10] Yin H, Wang L. Application and development prospect of digital twin technology in aerospace. *IFAC-PapersOnLine*. 2020;53(5):732–7. <https://doi.org/10.1016/j.ifacol.2021.04.165>.
- [11] Giering JE, Dyck A. Maritime Digital Twin architecture: A concept for holistic Digital Twin application for shipbuilding and shipping, at-Automatisierungstechnik 2021;69(12):1081–95. <https://doi.org/10.1515/auto-2021-0082>.
- [12] Opoku DGJ, Perera S, Osei-Kyei R, Rashidi M. Digital twin application in the construction industry: a literature review. *J Build Eng* 2021;40:102726. <https://doi.org/10.1016/j.jobe.2021.102726>.
- [13] Wanasinghe TR, Wroblewski L, Petersen BK, Gosine RG, James LA, De Silva O, et al. Digital twin for the oil and gas industry: overview, research trends, opportunities, and challenges. *IEEE Access* 2020;8:104175–97. <https://doi.org/10.1109/ACCESS.2020.2998723>.
- [14] Perno M, Hvam L, Haug A. Implementation of digital twins in the process industry: a systematic literature review of enablers and barriers. *Comput Ind* 2022;134:103558. <https://doi.org/10.1016/j.compind.2021.103558>.
- [15] Qi Q, Tao F, Hu T, Anwer N, Liu A, Wei Y, et al. Enabling technologies and tools for digital twin. *J Manuf Syst* 2021;58:3–21. <https://doi.org/10.1016/j.jmsy.2019.10.001>.
- [16] Lim KYH, Zheng P, Chen CH, Huang L. A digital twin-enhanced system for engineering product family design and optimization. *J Manuf Syst* 2020;57:82–93. <https://doi.org/10.1016/j.jmsy.2020.08.011>.
- [17] Negri E, Berardi S, Fumagalli L, Macchi M. MES-integrated digital twin frameworks. *J Manuf Syst* 2020;56:58–71. <https://doi.org/10.1016/j.jmsy.2020.05.007>.
- [18] Mroue H, Ramos JB, Wrobel LC, Jouhara H. Experimental and numerical investigation of an air-to-water heat pipe-based heat exchanger. *Appl Therm Eng* 2015;78:339–50. <https://doi.org/10.1016/j.aplthermaleng.2015.01.005>.
- [19] Lee S, Kang H, Kim Y. Performance optimization of a hybrid cooler combining vapor compression and natural circulation cycles. *Int J Refrig* 2009;32(5):800–8. <https://doi.org/10.1016/j.ijrefrig.2008.12.008>.
- [20] Wang Y, Yang C, Shen W. A deep learning approach for heating and cooling equipment monitoring. 2019 IEEE 15th International Conference on Automation Science and Engineering (CASE). IEEE; 2019. p. 228–34. <https://doi.org/10.1109/COASE.2019.8843058>.
- [21] Oh JS, Binns M, Park S, Kim JK. Improving the energy efficiency of industrial refrigeration systems. *Energy* 2016;112:826–35. <https://doi.org/10.1016/j.energy.2016.06.119>.
- [22] Du GE, Liebenberg L, Mathews EH, Du JN. A versatile energy management system for large integrated cooling systems. *Energy Convers Manag* 2013;66:312–25. <https://doi.org/10.1016/j.enconman.2012.12.016>.
- [23] Fong KF, Hanby VI, Chow TT. HVAC system optimization for energy management by evolutionary programming. *Energ Buildings* 2006;38(3):220–31. <https://doi.org/10.1016/j.enbuild.2005.05.008>.
- [24] Grieves M, Vickers J. Digital twin: mitigating unpredictable, undesirable emergent behavior in complex systems. *Transdisciplinary perspectives on complex systems: New findings and approaches* 2017;85–113. [https://doi.org/10.1007/978-3-319-38756-7\\_4](https://doi.org/10.1007/978-3-319-38756-7_4).
- [25] Schleich B, Anwer N, Mathieu L, Wartzack S. Shaping the digital twin for design and production engineering. *CIRP Ann* 2017;66(1):141–4. <https://doi.org/10.1016/j.cirp.2017.04.040>.
- [26] ISO/IEC. ISO/IEC 30173: 2023 digital twin: Concepts and terminology. Technical Report, <https://www.iso.org/standard/81442.html>; 2023.
- [27] Alves CA, Mauricio JM, Almeida RJSD, Azevedo IE. Digital twins of the water cooling system in a power plant based on fuzzy logic. *Sensors* 2021;21(20):6737. <https://doi.org/10.3390/s21206737>.
- [28] Tao F, Zhang M, Liu Y, Nee AY. Digital twin driven prognostics and health management for complex equipment. *CIRP Ann* 2018;67(1):169–72. <https://doi.org/10.1016/j.cirp.2018.04.055>.
- [29] Nguyen TN, Ponciroli R, Bruck P, Esselman TC, Rigatti JA, Vilim RB. A digital twin approach to system-level fault detection and diagnosis for improved equipment health monitoring. *Ann Nucl Energy* 2022;170:109002. <https://doi.org/10.1016/j.anucene.2022.109002>.
- [30] Ren Z, Wan J, Deng P. Machine-learning-driven digital twin for lifecycle management of complex equipment. *IEEE Trans Emerg Top Comput* 2022;10(1):9–22. <https://doi.org/10.1109/TETC.2022.3143346>.
- [31] Wei Y, Hu T, Yue P, Luo W, Ma S. Study on the construction theory of digital twin mechanism model for mechatronics equipment. *Int J Adv Manuf Technol* 2022;2022:1–19. <https://doi.org/10.1007/s00170-022-09144-w>.
- [32] ISO. ISO 23247-2:2021 automation systems and integration – Digital twin framework for manufacturing – part 2: Reference architecture. Technical Report, <https://www.iso.org/standard/75066.html>; 2021.
- [33] Kruger K, Human C, Basson A. Towards the integration of digital twins and service-oriented architectures. In: International workshop on service orientation in Holonic and multi-agent manufacturing. Springer; 2021. p. 131–43. [https://doi.org/10.1007/978-3-030-99108-1\\_10](https://doi.org/10.1007/978-3-030-99108-1_10).
- [34] O'Donovan P, Leahy K, Bruton K, O'Sullivan DT. An industrial big data pipeline for data-driven analytics maintenance applications in large-scale smart manufacturing facilities. *J Big Data* 2015;2(1):1–26. <https://doi.org/10.1186/s40537-015-0034-z>.
- [35] Lu Y, Liu C, Kevin I, Wang K, Huang H, Xu X. Digital Twin-driven smart manufacturing: Connotation, reference model, applications and research issues. *Robot, Comput-Integr Manuf* 2020;61:101837. <https://doi.org/10.1016/j.ircim.2019.101837>.
- [36] Yue C, Zhang Q, Zhai Z, Ling L. CFD simulation on the heat transfer and flow characteristics of a microchannel separate heat pipe under different filling ratios. *Appl Therm Eng* 2018;139:25–34. <https://doi.org/10.1016/j.aplthermaleng.2018.01.011>.
- [37] Lin Z, Wang S, Shirakashi R, Zhang LW. Simulation of a miniature oscillating heat pipe in bottom heating mode using CFD with unsteady modeling. *Int J Heat Mass Transf* 2013;57:642–56. <https://doi.org/10.1016/j.ijheatmasstransfer.2012.09.007>.
- [38] Ohrem SJ, Holden C. Modeling and nonlinear model predictive control of a subsea pump station. *IFAC-PapersOnLine* 2017;50:121–6. <https://doi.org/10.1016/j.ifacol.2017.12.022>.
- [39] Han Z, Xue D, Wei H, Ji Q, Sun X, Li X. Study on operation strategy of evaporative cooling composite air conditioning system in data center. *Renew Energy* 2021;177:1147–60. <https://doi.org/10.1016/j.renene.2021.06.046>.
- [40] Heiss JF, Coull J. Nomograph of dittrus-boelter equation for heating and cooling liquids. *Ind Eng Chem* 1951;43(5):1226–9. <https://doi.org/10.1021/ie50497a060>.
- [41] Shah MM. A general correlation for heat transfer during film condensation inside pipes. *Int J Heat Mass Transf* 1979;22(4):547–56. [https://doi.org/10.1016/0017-9310\(79\)90058-9](https://doi.org/10.1016/0017-9310(79)90058-9).
- [42] K-Space. K-space tutorial, version 4.8. Buskerud, Viken, Norway: Kongsberg Corp.; 2022. <https://www.kongsbergdigital.com/industrial-work-surface/kognitwin-k-space>.
- [43] Komulainen TM, Enmark-Rasmussen R, Sin G, Fletcher JP, Cameron D. Experiences on dynamic simulation software in chemical engineering education. *Educ Chem Eng* 2012;7(4):153–62. <https://doi.org/10.1016/j.ece.2012.07.003>.
- [44] Zhang Q, Meng Z, Hong X, Zhan Y, Liu J, Dong J, et al. A survey on data center cooling systems: technology, power consumption modeling and control strategy optimization. *J Syst Archit* 2021;119:102253. <https://doi.org/10.1016/j.jsysarc.2021.102253>.
- [45] Pujol J. The solution of nonlinear inverse problems and the Levenberg-Marquardt method. *Geophysics* 2007;72(4):1–16. <https://doi.org/10.1190/1.2732552>.
- [46] Gavin HP. The Levenberg-Marquardt algorithm for nonlinear least squares curve-fitting problems. Department of civil and environmental engineering, Duke University; 2019. 19, <https://people.duke.edu/~hpgavin/ExperimentalSystem/slm.pdf>.